Modeling Species-Specific Collision Risk of Birds with Wind Turbines: A Behavioral Approach

Linder, Anne Cathrine; Lyhne, Henriette ; Laubek, Bjarke ; Bruhn, Dan; Pertoldi, Cino

Published in:
Symmetry

DOI (link to publication from Publisher):
10.3390/sym14122493

Publication date:
2022

Document Version
Publisher's PDF, also known as Version of record

symmetry

MDPI

Article

Modeling Species-Specific Collision Risk of Birds with Wind Turbines: A Behavioral Approach

Anne Cathrine Linder [1,2,*], Henriette Lyhne [2], Bjarke Laubek [3], Dan Bruhn [2,4] and Cino Pertoldi [2,5]

1 National Institute of Aquatic Resources, Technical University of Denmark, 2800 Kongens Lyngby, Denmark
2 Department of Chemistry and Bioscience, Aalborg University, 9220 Aalborg, Denmark
3 Vattenfall Renewable Wind DK A/S, 6000 Kolding, Denmark
4 Skagen Bird Observatory, 9990 Skagen, Denmark
5 Aalborg Zoo, 9000 Aalborg, Denmark
* Correspondence: acali@aqua.dtu.dk

Abstract: The increasing number of wind energy sites developed globally, has consequently resulted in a green-on-green predicament, due to an increase in avian mortality caused by collisions with wind turbines. The proportion of collision-related fatalities is not evenly distributed across species, indicating that some species groups are more prone to turbine collision. Such differences between species have been proposed to be affiliated with species-specific foraging and flight behavior. The aim of this study is to investigate how the flight behavioral traits; head position, active flight, track symmetry, and track tortuosity can be used to model collision risk along with other influencing factors i.e., weather variables (temperature, wind speed, and cloud coverage) and temporal variables (time of day and time of year). The study also sought to investigate the species-specificity of the four traits in relation to the phylogenetic relatedness of the study species. This was achieved through a case study at a wind farm on the Swedish island of Gotland in which the behavior of birds from 11 different genera was studied. The flight behavior of these species was assessed using data collected by the IdentiFlight system, e.g., flight trajectories and images of the birds throughout their flight track. The results confirm the species-specificity of the four flight behaviors and indicated that all four traits can be used to predict collision risk along with species as a categorical factor. The framework provided in this study along with the results of the case study can be used to identify risk-prone species based on phylogenetic relatedness and flight behavior.

Keywords: collision risk; IdentiFlight; wind turbine curtailment; phylogenetic signal; flight behavior; flight symmetry

Citation: Linder, A.C.; Lyhne, H.; Laubek, B.; Bruhn, D.; Pertoldi, C. Modeling Species-Specific Collision Risk of Birds with Wind Turbines: A Behavioral Approach. *Symmetry* **2022**, *14*, 2493. https://doi.org/10.3390/sym14122493

Academic Editor: John H. Graham

Received: 5 August 2022
Accepted: 24 October 2022
Published: 24 November 2022

1. Introduction

The growing demand for green energy has resulted in the rapid development of wind energy production, yielding an increasing number of wind turbines globally. This has in turn led to a green-on-green predicament, due to the adverse effects of turbines on many avian species [1–9]. These adverse effects of wind turbines on birds result primarily from direct fatalities due to collisions and secondarily through habitat alteration and loss [9]. The precise number of avian collisions with wind turbines is uncertain, but even relatively few fatalities can have detrimental effects on slow maturing species with low reproduction rates, particularly for species of conservation concern when considering regional and national populations [1,7]. Collision-related mortality is unevenly spread among species, with a few species often accounting for a large proportion of collision victims [10]. Large soaring raptors are known to be specifically vulnerable to collision with turbines [2,3,9,11]. Other species groups prone to collision fatalities at wind farms include herons, geese, and gulls [10,11].

Differences between species in regard to their susceptibility to turbine collisions are suggested to be associated with species-specific foraging behavior, flight behavior, and mor-

phology [1,3,12]. In some species, e.g., raptors and cranes, particularly vulnerable to collisions, their visual field is such that even a small (25–35°) forward pitch head movement will leave them blind directly ahead [13]. Thus, the foraging behavior of many raptors may explain why these species are more prone to turbine collisions. Many raptor species forage from the air, by bending their heads and looking downwards to search for prey or carrion on the ground [14]. Raptors that hunt terrestrial prey have a large blind spot above their head, which functions to avoid sun dazzling, thus, allowing for better prey detection. However, this blind spot also renders these raptors blind in their travel direction whilst foraging [13,14].

Morphological differences between species have also been proposed to attribute to species-specific differences in collision fatalities, where birds with high wing loading, i.e., the ratio between a bird's total mass and wing area, and relatively large bodies, e.g., cranes (*Grus* spp.), are suggested to be more vulnerable to turbine collision due to reduced maneuverability and rapid flight speeds [15–17]. Morphological differences between species may also impact how different species are affected by various weather conditions. It has been suggested that herons (*Ardea* spp.) and other species with a slow and ponderous flight can more easily be buffeted off course during strong headwinds, thus, making them vulnerable to turbine collision when flying between roosts and foraging sites [18]. Furthermore, many large raptors utilize thermal soaring, i.e., slow circle-soaring flight on thermals. This flight strategy is highly dependent on weather conditions, e.g., temperature and cloud coverage, and under less favorable conditions for gaining altitude thermal soaring may impact turbine collision risk [12,19–21]. Turbine collision risk has also been found to differ throughout the day and throughout the year [20,22].

Species-specific differences in flight behavior and collision risk may also be correlated with phylogenetic relatedness of species. This correlation can be quantified by the phylogenetic signal of each trait. The phylogenetic signal can be defined as the tendency for closely related species to resemble one another more than species drawn at random from the phylogenetic tree [23]. A phylogenetic signal will occur if traits evolve in a Brownian motion-like manner, i.e., relatively small changes occur randomly in any given direction over time independent of the former state of the trait. This pattern of evolution can arise from genetic drift or natural selection [24,25]. Hence, the phenotypic difference can be expected to be smaller between species who shared a common ancestor more recently [24,26]. For a trait that changes gradually over time, the covariance between species' trait values is expected to be proportional to the shared evolutionary history between species, i.e., the sum of the species' shared branch length in a phylogenetic tree. Furthermore, the variance of a trait value for a given species is expected to be proportional to the total length of the tree for that species, i.e., the summed branch length from the root to the tip [25].

Herrera-Alsina et al. [27] used a similar phylogenetic approach to study species-specific collision risk in relation to the species' morphological differences and phylogenetic relationship, finding a correlation between wing loading and the likelihood of flight in the risk zone. However, it is more difficult to assess species-specific differences in flight behavior associated with collision risk, as flight behavior can be difficult to observe and quantify, particularly in relation to flight in close proximity to wind turbines (within a 100 m radius from the nearest turbine's rotor tip), i.e., in collision risk zones [28]. The relationship between species-specific behavioral traits and turbine collision risk is, therefore, often based on assumptions. However, the development of automated camera-based monitoring systems, e.g., IdentiFlight, has effectuated the collection of large amounts of behavioral data within wind farms [29,30]. The IdentiFlight system was developed to mitigate the impact of wind turbines on species of conservation concern, by detecting birds in flight and curtailing turbines if a protected species is at collision risk [29,30]. The utilization of bird images and flight trajectories collected by the IdentiFlight system, to assess flight behavior, has recently been demonstrated and the quantitative flight behavioral traits head position, active flight, track tortuosity, and track symmetry described by Linder et al. [28] can possibly be used to model collision risk.

The aim of this study was, therefore, to investigate how the flight behavioral traits; head position, active flight, track tortuosity, and track symmetry can be used to model collision risk along with other influencing factors, i.e., the weather variables; temperature, wind speed, and cloud coverage, and the temporal variables; time of day, and time of year. This was achieved through a case study investigating the behavior of birds from 11 different genera (*Anser*, *Ardea*, *Aquila*, *Buteo*, *Corvus*, *Grus*, *Haliaeetus*, *Milvus*, *Larus*, *Pandion*, and *Phalacrocorax*) at a wind farm located on the Swedish island Gotland. The flight behavior of these species was assessed using data collected by the IdentiFlight system, e.g., flight trajectories and images of the birds throughout their track. It was expected that collision risk could be predicted by species, flight behavior, weather variables, and temporal variables. More specifically, collision risk was expected to increase with time spent looking down and an increase in tortuosity. Moreover, increased utilization of active flight was expected to decrease collision risk. This study will also investigate whether the four flight behavioral traits and thereby collision risk are species-specific, and if such species-specificity is due to random effects (lack of evolutionary signal) or shared evolutionary history (significant evolutionary signal). This was achieved by assessing the phylogenetic signal, i.e., the tendency of related species to resemble each other more than species randomly drawn from the same phylogenetic tree, for the four behavioral traits (head position, active flight, track symmetry, and track tortuosity). The behavioral trait head position was expected to be species-specific in relation to the species' foraging ecology and the active flight was expected to be species-specific in relation to the species' morphological differences. Track symmetry and tortuosity were expected to be species-specific as a result of both foraging ecology and morphology. These expected species-specific differences in behavioral traits were expected to be correlated with phylogenetic relatedness.

2. Materials and Methods

2.1. Study Site

The study site is located on Näsudden, a peninsula on Gotland's southwest coast where the terrain is generally flat [31]. The entire wind farm consists of 55 turbines, with differing heights from 45–145 m [28]. The observational area of the study site was defined by a 400 m radius around the IdentiFlight camera tower, including nine wind turbines (Appendix A).

2.2. Study Species

Gotland is home to a large number of bird species and is also visited by various migrating species. Some of the species living on Gotland include breeding populations of approximately 55 golden eagle (*Aquila chrysaetos*) pairs, 45 white-tailed eagle (*Haliaeetus albicilla*) pairs, and 15 red kite (*Milvus milvus*) pairs [32,33]. Other avian species on Gotland include grey heron (*Ardea cinerea*), western osprey (*Pandion haliaetus*), black kite (*Milvus migrans*), common crane (*Grus grus*), great cormorant (*Phalacrocorax carbo*), common buzzard (*Buteo buteo*), as well as several goose (*Anser*), gull (*Larus*) and crow (*Corvus*) species. The only goose species included in this investigation is the graylag goose (*Anser anser*) as there were not enough observations of other goose species. Furthermore, the genera crow and gull each consist of multiple species, as the image quality made it difficult to distinguish between the different species within each genus. The study species represent eight different families. The general term raptors, as used in this study, is used in reference to the order Accipitriformes, which includes the following species: golden eagle, white-tailed eagle, western osprey, red kite, black kite, and common buzzard.

2.3. Data Collection

Observations of the selected study species were collected by the IdentiFlight camera system [30] over a 13-month period from the middle of February 2020 to the end of March 2021. The camera system is developed to initiate turbine curtailment when individuals of the species; golden eagle, white-tailed eagle, or red kite, are within a predefined distance of one of the nine turbines covered by the system (Appendix B). However, at the time of the

study, the system was still being trained. This resulted in a large number of false positives, i.e., other bird species wrongfully classified as the golden eagle, white-tailed eagle, or red kite, which effectuated the collection of data for multiple other bird species. During the study period, the IdentiFlight system was only collecting simulated curtailment data for the nine turbines, hence, the system was not actively curtailing turbines. Throughout this period of time, the system was periodically out of operation and the study is therefore based on a total of 375 days over the course of these months with bird sightings within the observational zone on only 296 of these days (Appendix C).

2.3.1. IdentiFlight System

The IdentiFlight system consists of eight wide field-of-view cameras fixed in a ring, and a single high-resolution stereo camera mounted on top of a six-meter tower (Appendix B). The eight wide field of view cameras uses image sensor arrays to detect moving objects in the environment and begin to track them [28]. These cameras collect ten images per second. Upon detecting a moving object the movable high-resolution stereo camera is directed at the object. This camera collects approximately one image per second and uses high-magnification stereoscopic sensors to determine the distance to the object and gather the necessary information to classify the object. IdentiFlight's computer vision algorithms use a catalog of rules to analyze the images obtained by the high-resolution stereo camera [28]. The IdentiFlight system collects a large variety of variables along with an image of the bird for each observation. A unique track ID is assigned to each track and annotated for each observation throughout the track. For each observation the time, date, and bird's geographical position are collected [28]. Furthermore, flight trajectories for each track are saved as Keyhole Markup Language (KML: a file format used to display geographic data) files, that can be imported into ArcGIS Pro for further analysis [34].

2.3.2. Weather Data

Temperature, wind speed, and cloud coverage were measured in hourly intervals by the Swedish Meteorological and Hydrological Institute at a weather station near the study site approximately 34 m above sea level [35].

2.4. Data Preparation

The species of each track was determined manually, by the two authors, based on the bird images. The bird images were also used to classify the head position of each bird, i.e., oriented straight forward or down towards the ground, and whether the bird was utilizing active flight, i.e., flapping its wings, throughout its track (Figure 1). Classifications of head position and active flight were completed for each observation within 400 m of the camera tower, as it was difficult to classify the head orientation of the bird for images taken at further distances. This resulted in a data set of 887 different tracks of the various species based on 30,007 observations (Appendix D).

The flight trajectories (KML files) were analyzed using ArcGIS Pro [34]. For each flight trajectory the track symmetry, i.e., the summed angles of directional changes, and tortuosity, i.e., the ratio between the direct track length and the actual track length, were calculated using the ArcPy package in Esri [34] (Appendix E). The track angles distinguished between left and right turns, thus, ranging from -180° to 180°.

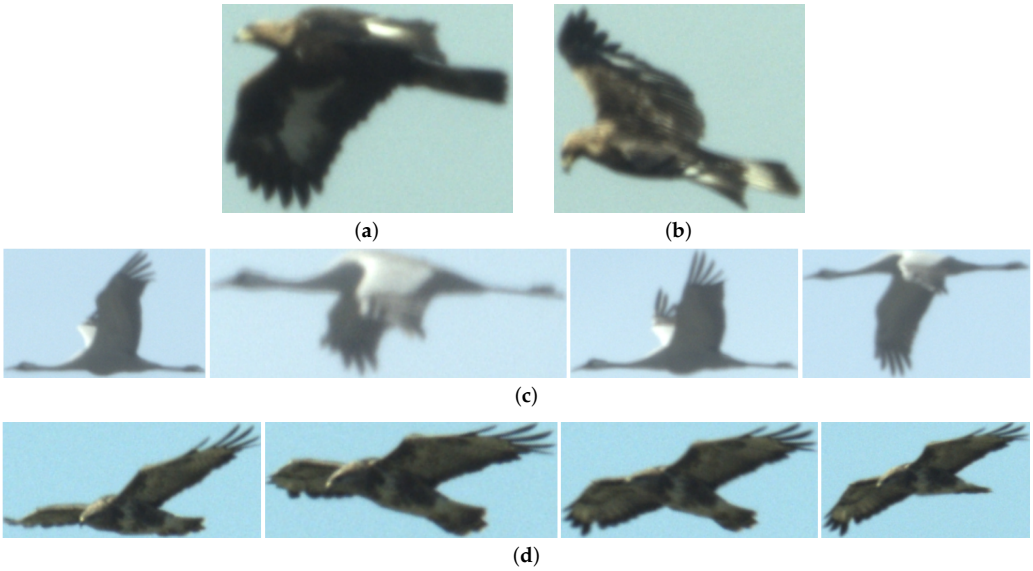

Figure 1. Examples of how the birds' behavior was scored based on images. Head position was classified from a single image while active flight had to be classified from a series of images in order to evaluate the bird's wing movement between images. (**a**) A golden eagle with its head oriented straight. (**b**) A golden eagle with its head oriented down. (**c**) A series of images showing a Eurasian crane flapping its wings, i.e., in active flight. (**d**) A series of images showing a common buzzard soaring, i.e., not in active flight.

2.5. Data Analysis

Collision risk was quantified as the proportion of time an individual spent in the defined risk zone (Figure 2). The collision risk zone was defined as a sphere where the radius was the length of the rotor blade plus 100 m around each wind turbine meaning the collision risk zone depended on turbine size.

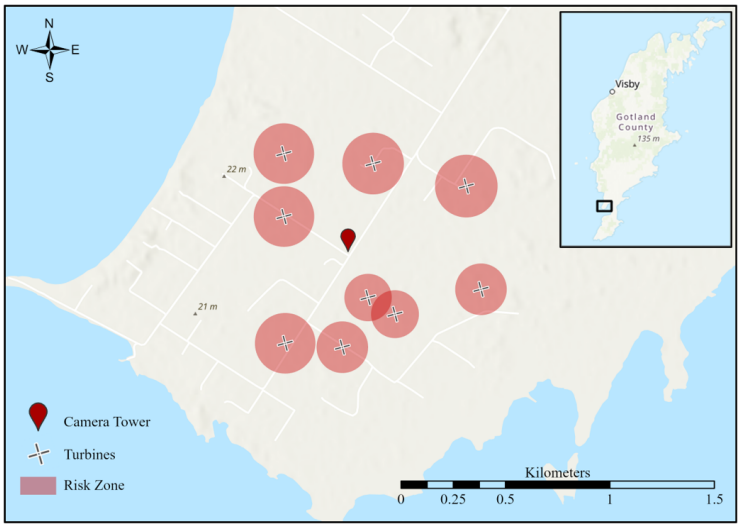

Figure 2. Risk zone around the turbines (Appendix F).

Both univariate and multivariate analyses were conducted to describe the relationship between the possible explanatory variables and collision risk as the response variable (Table 1). Furthermore, phylogenetic signals were calculated to determine if closely related species exhibited similar flight traits regarding flight symmetry and flight tortuosity as well as head position during flight and proportion of time spent in active flight. All statistical analyses were conducted in R version 4.0.3 [36].

Table 1. Variables used in the data analysis.

Variable	Description	Type
Risk proportion	Proportion of time spent in collision risk zone	Response variable
Species	Bird species	Categorical covariate
Head position	Proportion of observations looking down	Continuous covariate
Active flight	Proportion of observations spent on active flight	Continuous covariate
Track symmetry	Absolute sum of track angles	Continuous covariate
Track tortuosity	Track length ratio (proportion between 0 and 1)	Continuous covariate
Cloud coverage	Cloud cover as a percentage	Continuous covariate
Temperature	Temperature in °C	Continuous covariate
Wind speed	Wind speed in m/s	Continuous covariate
Time of year	Month (mo) from February to August	Continuous covariate
Time of day	Time (h)	Continuous covariate

2.5.1. Univariate Predictions of Collision Risk

General species-specific differences in flight behavior and collision risk, were investigated by summarizing species-grouped data. Graphs were created for the covariates; head position, active flight, track symmetry, and track tortuosity, and also for the response variable to depict the median and interquartile range (25–75%) for each species. The relationship between the response variable and each covariate was assessed individually in a simple regression analysis and quantified by the coefficient of determination (R^2). This analysis was conducted with all species pooled, raptor species pooled, and each species individually. Furthermore, subsets termed risk tracks were created including only tracks with a proportion of time spent in the risk zone greater than zero, due to the large number of zeros in the data set. The individual relationships between the response variable and covariates were then assessed for all tracks in the risk zone (all risk tracks), raptors in the risk zone (raptor risk tracks), and each species' tracks in the risk zone, individually (species risk tracks).

2.5.2. Modeling Collision Risk

A preliminary data exploration was used to select the explanatory variables for the multivariate analysis [37]. To assess collinearity Spearman's correlation coefficient (r) was calculated among the covariates and pairwise scatter-plots were created to detect obvious correlations among the covariates (Appendix G.2). Furthermore, a variance inflation factor (VIF) analysis was performed to identify collinearity (Appendix G.1). In this analysis VIF values higher than 2 meant that the predictor with the highest VIF was sequentially dropped and VIF values were recalculated [37]. This analysis resulted in the variables temperature and flight symmetry being excluded from the multivariate analysis due to collinearity. Thus, the possible explanatory variables used in the model selection were head position, active flight, flight tortuosity, species, wind speed, cloud coverage, time of year, and time of day. Automated multivariate model selection, using the R package glmulti [38] was used to assess the importance of each covariate. In the automated model selection all possible models were fitted and the best model was selected according to prediction error using the Akaike information criterion (AIC) [37]. The automated model selection was carried out for models both with and without interactions for all tracks, raptor tracks, all risk tracks, and raptor risk tracks. For each subset the models with and without interactions were compared based on their respective AIC values. Moreover, an Anova test using the χ^2 test statistic was also used to assess the goodness of fit of the nested regression models, i.e., the models with and without interactions [39]. The model with interactions was selected as the best model if the addition of interaction terms significantly increased the model's goodness of fit, if not the simpler of the two models, i.e., the model without interactions, was selected. Furthermore, the estimated importance of model terms was estimated using the sum of Akaike evidence weights of all models in which the term appears. The relative importance of model terms, ranging between 0 and 1, can be used to

identify covariates that significantly contribute to explaining the variation of the response variable, using a threshold of 0.8. This threshold is based on type I and II statistical risks, i.e., the probability of retaining a non-important term (type I error) and the probability of disregarding an important term (type II error) [38].

2.5.3. Phylogenetic Signal

Evolutionary analyses were conducted in MEGA X (Molecular Evolutionary Genetics Analysis across computing platforms) [40]. The phylogenetic tree was created using the Maximum Likelihood method and the Tamura-Nei model [41]. The reliability of the tree was tested by bootstrapping the tree ten thousand times. Branches with bootstrap values above 70% are expected to define a true clade within the tree whereas branches with values under 30% are expected to show an incorrect clade [42]. The evolutionary history between the selected bird species was based on the mitochondrial gene cytochrome c oxidase I (COX1) as it is the mitochondrial gene with the least variation among aves orders and at the same time have the lowest amount of heterogeneity across lineages, i.e., different mutations in the gene can cause highly different phenotypes [43]. The sequences were downloaded from GenBank [44] and aligned by Multiple Sequence Comparison by Log-Expectation (MUSCLE) in MEGA X. MUSCLE implements a progressive algorithm that re-optimizes alignments during the whole alignment process, making it possible to correct wrong alignments made at the beginning of the process [45]. The phylogenetic signal can be defined as the degree to which variations in species' trait values are predicted by the relatedness among species. The phylogenetic signal was evaluated by calculating Blomberg's K statistic [23,46]. The behavioral traits (proportion frames spent looking down, proportion frames spent on active flight, flight symmetry, and flight tortuosity) were selected for this analysis.

3. Results

3.1. General Flight Behavior of Each Species

Raptors in general had more asymmetric and tortuous tracks than the other bird species (Figure 3a,b). It was clear that buzzards had the most asymmetric ($median = 503$, IQR = 148–1124) and tortuous ($median = 0.507$, IQR = 0.372–0.717) tracks. Furthermore, raptors generally had a large variation (IQR) within the single species in both track symmetry and tortuosity, compared to that of the other bird species. Raptors also spent a relatively large proportion of frames looking down ($median > 0.5$), where red kite was the species that spent the largest proportion of frames looking down ($median = 0.909$, IQR = 0.776–1.00) (Figure 3c). White-tailed eagles ($median = 0.333$, IQR = 0.00–0.714), western osprey ($median = 0.417$, IQR = 0.0833–0.675), and golden eagles ($median = 0.112$, IQR = 0.00–0.304) were the only raptors generally engaging in active flight i.e., all other raptors spent less than 15% of frames on active flight ($median < 0.12$) (Figure 3d). The birds generally spent little time in the defined collision risk zone, i.e., no species had a median risk proportion above 0.0540 (Figure 3e). Nonetheless, a large proportion of the birds intersected the risk zone at one point or another throughout their track, particularly white-tailed eagles (48.3% of all tracks) (Figure 4).

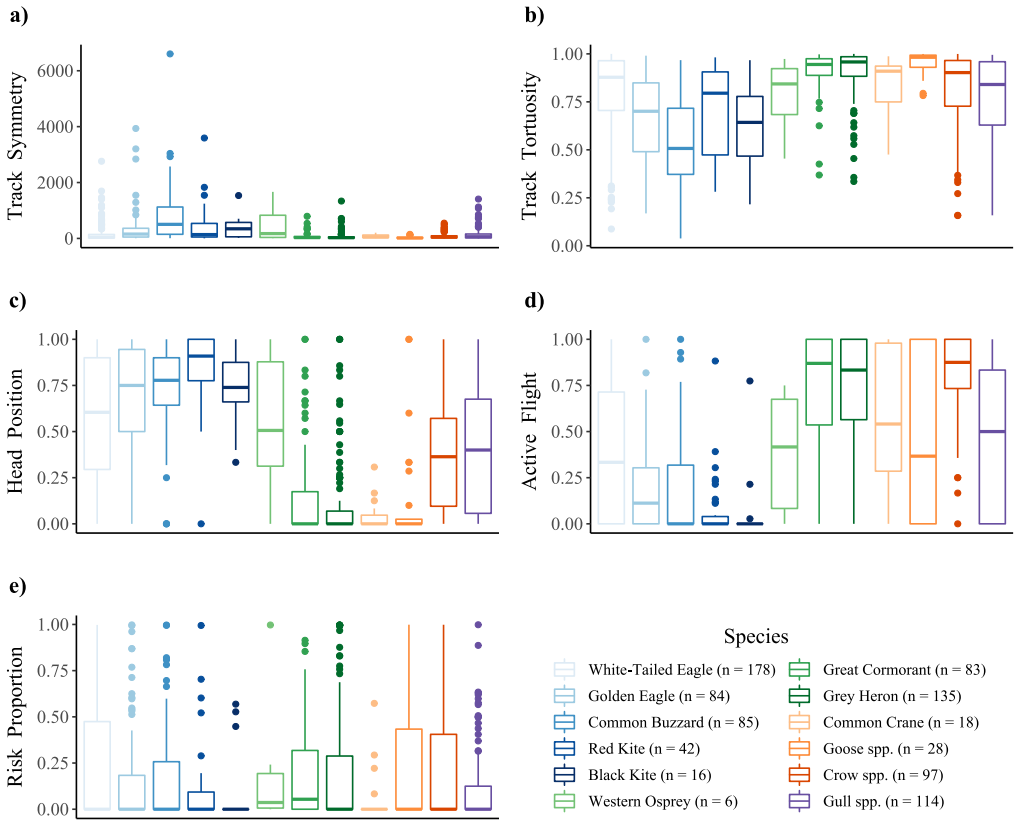

Figure 3. Distribution of each variable grouped by species. The number of tracks for each species is annotated in the legend beside the species name. (**a**) Track symmetry i.e., the absolute sum of directional changes where a value of zero indicates a completely symmetrical track. (**b**) Track tortuosity as the ratio between the shortest distance from a track's start to the endpoint, and the actual track length i.e., a lower ratio represents a more tortuous track. (**c**) Head position as the proportion of frames spent looking down throughout a track. (**d**) Active flight as the proportion of frames spent in active flight throughout a track. (**e**) Risk proportion i.e., the proportion of time spent in the defined collision risk zone throughout a track.

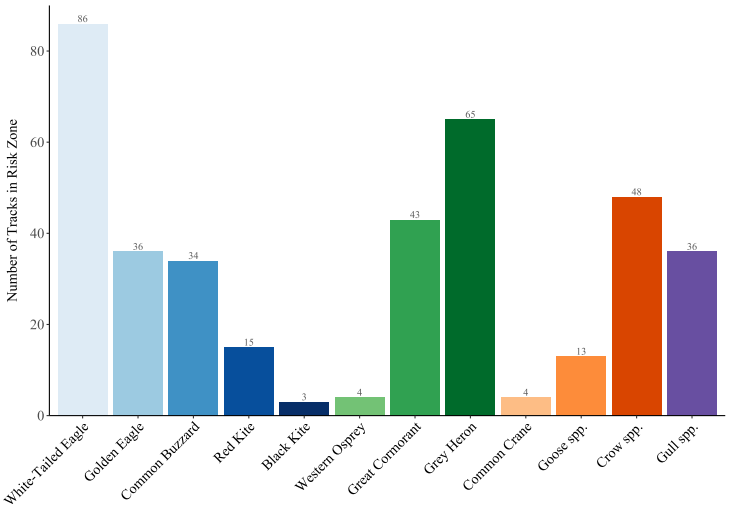

Figure 4. Number of tracks for each species that at some point enter the risk zone. The number of tracks is annotated above each bar.

3.2. Predicting Collision Risk

When assessing all tracks collectively, there were no significant relationships between the response variable, proportion of time spent in the risk zone, and the individual covariates (Appendix H). This was also the case when assessing the relationship for each individual species' tracks, with the exception of white-tailed eagle and gull spp. tracks.

For white-tailed eagle tracks there was a significant but weak negative relationship between head position and the collision risk ($R^2 = 0.0220, p < 0.05$) and between temperature and collision risk ($R^2 = 0.0428, p < 0.01$) (Appendix H). For all raptor tracks there was a significant relationship between collision risk and the respective covariates, head position ($R^2 = 0.0181, p < 0.01$) and temperature ($R^2 = 0.0163, p < 0.01$). When assessing only tracks in the risk zone the relationship between the response variable and some of the covariates was more apparent, particularly when focusing on the raptor species. A significant but weak relationship was found between collision risk and the respective covariates, track symmetry ($R^2 = 0.0217, p < 0.05$), track tortuosity ($R^2 = 0.02785, p < 0.001$), and time of day ($R^2 = 0.0119, p < 0.05$) (Figure 5). The relationship between collision risk and track tortuosity became clearer when the assessment only accounted for raptor tracks in the risk zone, showing that track tortuosity was a relatively strong significant predictor of risk ($R^2 = 0.101, p < 0.001$) (Figure 6). Moreover, there was a significant relationship between collision risk and active flight for raptor tracks in the risk zone ($R^2 = 0.0320, p < 0.05$).

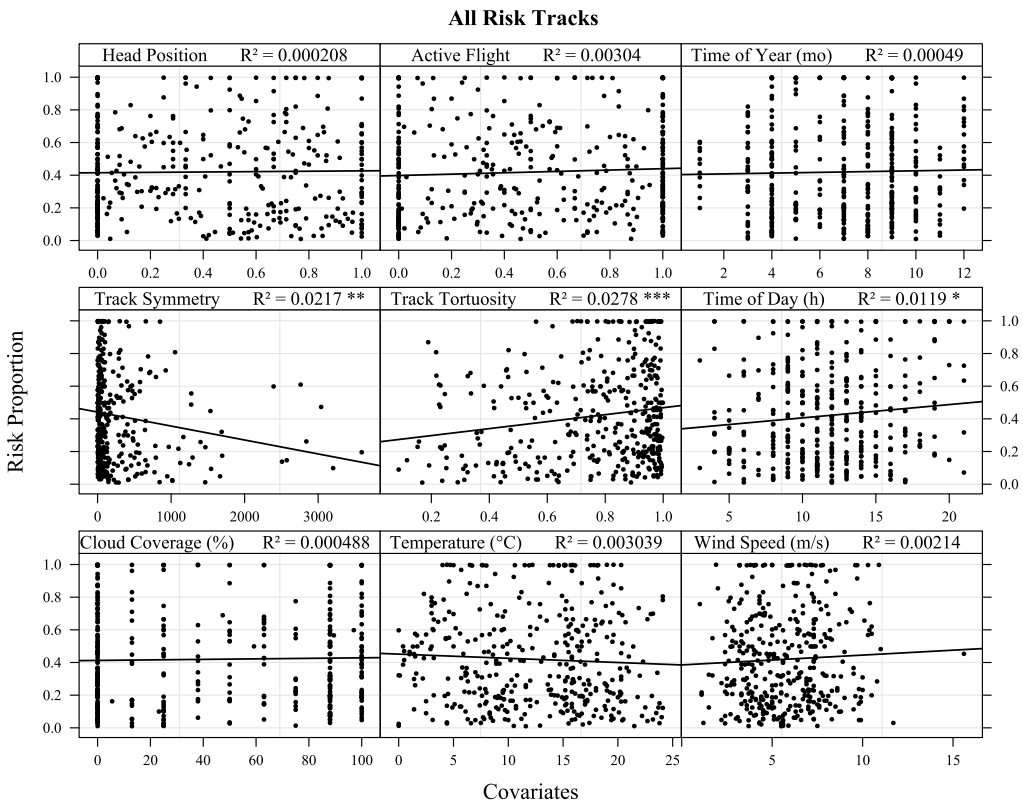

Figure 5. Proportion time spent in risk zone as a function of each possible explanatory variable for all risk tracks, i.e., all species tracks that intersected the risk zone. A regression trend line is depicted for each plot along with the coefficient of determination (R^2) and significance level (* $p < 0.05$, ** $p < 0.01$, *** $p < 0.001$).

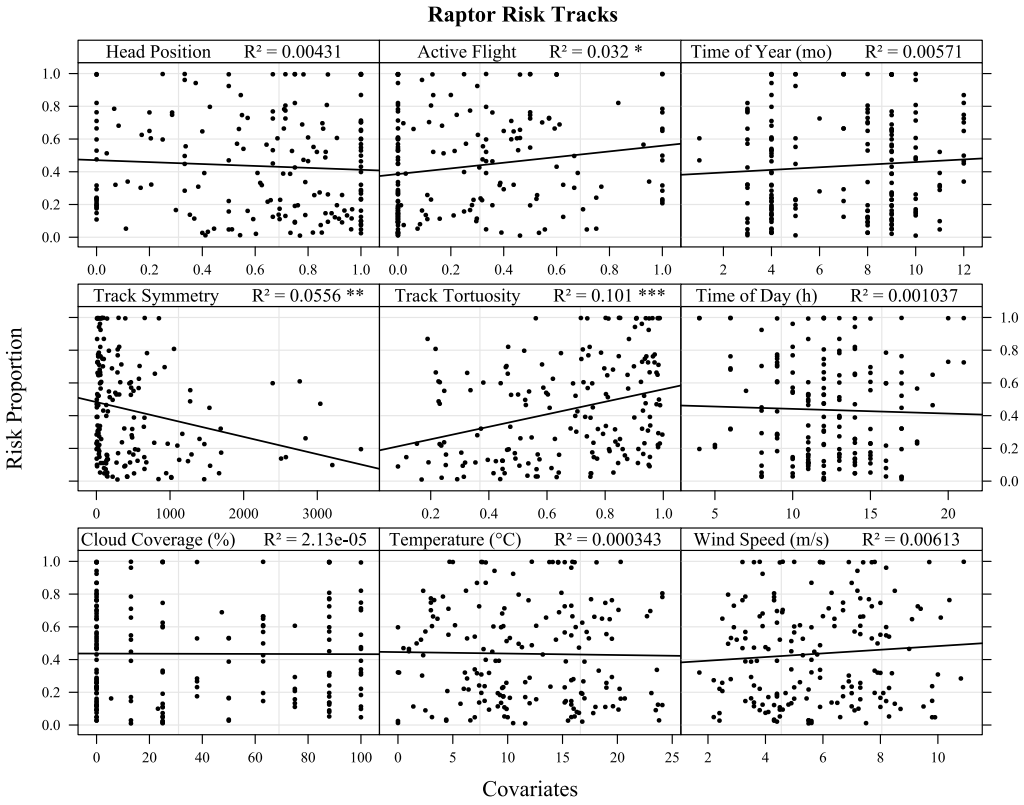

Figure 6. Proportion time spent in risk zone as a function of each possible explanatory variable for raptor risk tracks, i.e., raptor tracks that intersected the risk zone. A regression trend line is depicted for each plot along with the coefficient of determination (R^2) and significance level (* $p < 0.05$, ** $p < 0.01$, *** $p < 0.001$).

Collision Risk Models

The comparison of models with and without interactions indicated the simpler of the two models to be the better choice for all tracks, all risk tracks, and raptor risk tracks. For raptor risk tracks the addition of interaction terms significantly improved the model's goodness of fit (Appendix I). The automated model selection without interactions for all tracks indicated that species (evidence weight = 0.962) was the most important model term, and the only covariate that significantly contributed to explaining the variation of the response, as it was the only covariate with an evidence weight over the threshold of 0.8 (Figure 7a). Whereas, active flight × wind speed (evidence weight = 0.994), cloud coverage × time of year ((evidence weight = 0.993), active flight × time of year (evidence weight = 0.985), time of year × species (evidence weight = 0.973), species (evidence weight = 0.973), cloud coverage × wind speed (evidence weight = 0.959), head position (evidence weight = 0.926), and cloud coverage × time of day (evidence weight = 0.919) were the most important model terms for the model selection for raptor tracks with interactions (Figure 7b). When excluding tracks outside the risk zone the automated model selection without interactions for all species tracks indicated that tortuosity (evidence weight = 1.00), and time of day (evidence weight = 0.853) were the two covariates that significantly contributed to explaining the variation of the response (Figure 7c). When considering only raptor tracks in the risk zone tortuosity (evidence weight = 1.00) was the single most important model term, and the only covariate with an evidence weight over the threshold in the model selection without interactions (Figure 7d). It should be emphasized that the absolute results from the collision risk models should only be interpreted as indications and should not be taken literally.

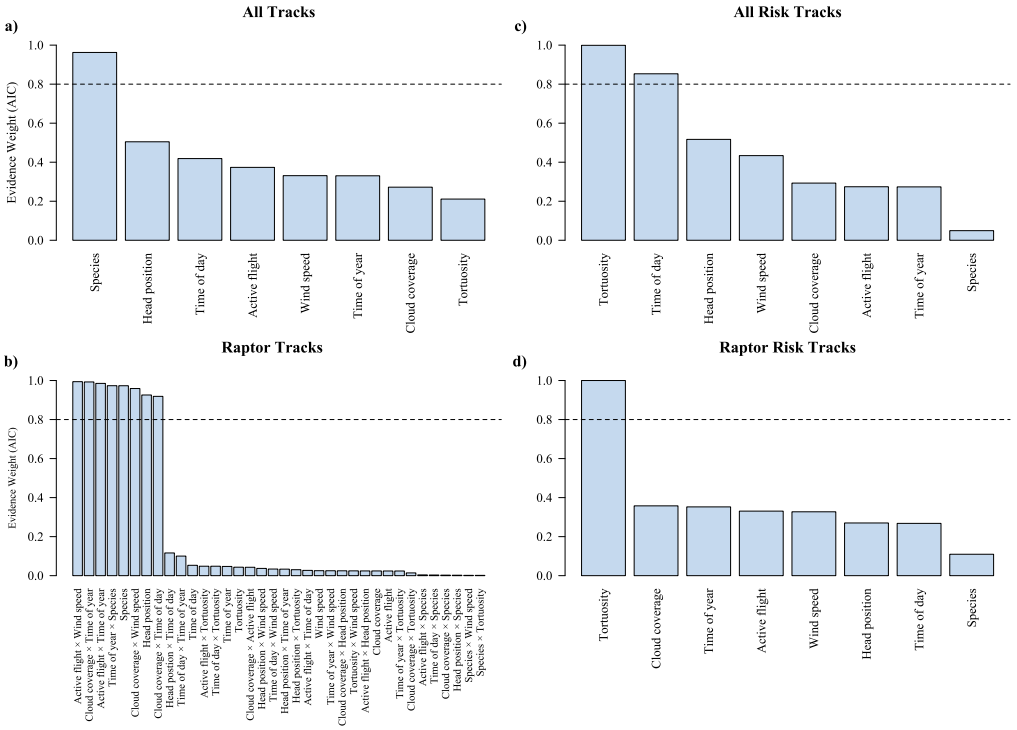

Figure 7. Relative importance of each model term for (**a**) all species tracks without interactions, (**b**) raptor tracks with interactions, (**c**) all tracks in the risk zone without interactions, and (**d**) only raptor tracks in the risk zone without interactions. Each term's relative importance was estimated with the automated model selection as the sum of Akaike evidence weights of all models in which the term appears.

3.3. Species-Specificity of Flight Behavioral Traits

The phylogenetic analysis indicated that the flight behavior of closely related species, such as red kites and black kites, resembles each other more than that of species randomly drawn from the tree (Figure 8). More specifically, the three behavioral traits, head position ($K = 1.64, p = 0.002$), active flight ($K = 1.83, p = 0.002$), and track symmetry ($K = 1.05, p = 0.047$), exhibited statistically significant levels of phylogenetic signal, with *K*-values greater than 1 (Figure 9). For the trait, track tortuosity ($K = 0.939, p = 0.045$), the phylogenetic signal was not stronger than expected under Brownian motion, with a *K*-value under the threshold of 1 (Figure 9).

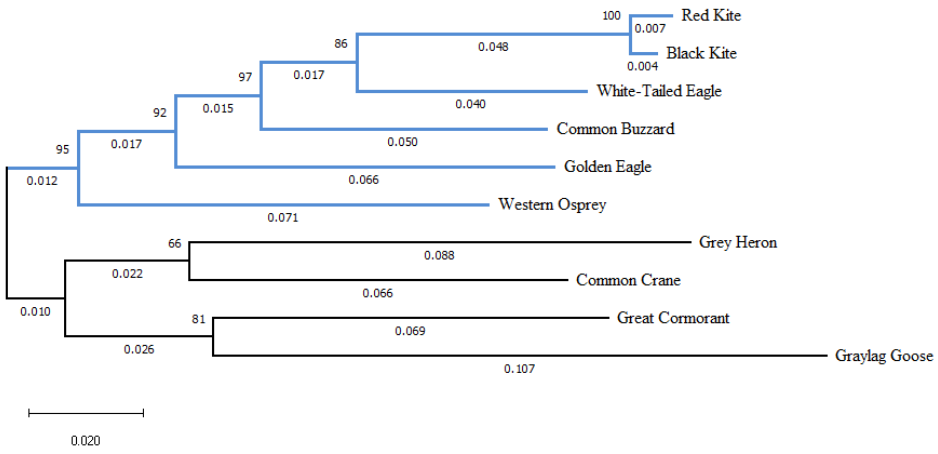

Figure 8. Evolutionary history between the selected bird species. Branch length values are noted under each branch and bootstrap values (%) above the branches. Blue branches represent raptor species.

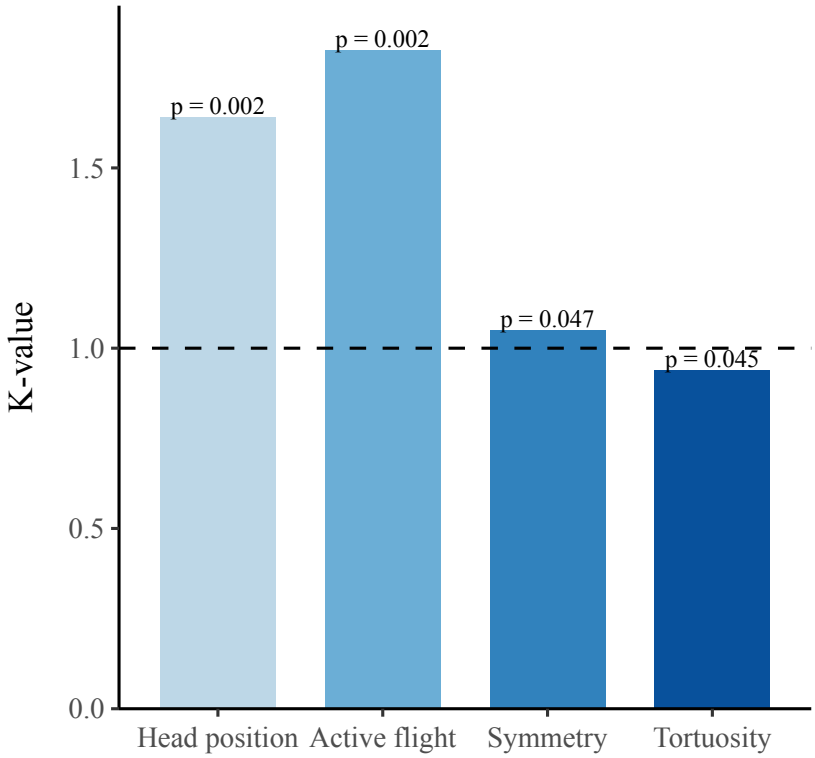

Figure 9. Phylogenetic signal in flight behavior traits using *K*. The horizontal dotted line represents a *K*-value of 1, which indicates a strong phylogenetic signal that follows Brownian motion perfectly. *K*-values above this line indicate phylogenetically conserved traits.

4. Discussion

4.1. Flight Behavior as a Predictor of Collision Risk

Track tortuosity was found to be an important predictor of collision risk, with an evidence weight = 1.00 for risk tracks and raptor risk tracks (Figure 7). The univariate analysis also indicated a significant but weak relationship between track tortuosity and collision risk for all tracks in the risk zone ($R^2 = 0.0278, p < 0.001$) (Figure 5). This relationship was more apparent for raptor tracks in the risk zone ($R^2 = 0.101, p < 0.001$), with the relationship being strongest for golden eagle tracks in the risk zone ($R^2 = 0.138, p < 0.01$) (Figures 6 and A23). This association between collision risk and tortuosity indicated that higher collision risk was associated with less tortuous tracks for raptor species in the case study. Thus, disproving the hypothesis that more tortuous tracks yield a higher collision risk and contradicting the same assumption made by Linder et al. [28]. Tortuous tracks can be a result of birds utilizing thermal soaring, as shown by the results of Linder et al. [28], hence, collision risk was reduced when the birds utilized thermal soaring. This is in agreement with Peron [47] and Janss [15] who found that collision risk was lowest for birds utilizing thermal soaring. Active flight was also weighted as a relatively important risk predictor for raptor tracks, in the automated model selection, with an evidence weight > 0.85 (Figure 7b). The univariate analysis for raptor tracks showed increased active flight to be a significant but weak predictor of increased collision risk ($R^2 = 0.0116, p < 0.05$) (Figure A11). Thus, contradicting the initial expectation that increased utilization of active flight would result in a low collision risk, but further confirming the previous result that less tortuous tracks increase collision risk, as Linder et al. [28] found that high utilization of active flight was associated with a low track tortuosity. Moreover, the results indicate a general tendency in which species with low track tortuosity had a high utilization of active flight, e.g., grey heron and great cormorant (Figure 3b,c). However, for the individual non-raptor species, there were no significant relationships between these two respective predictor variables and collision risk (Appendix H).

The relationship between the active flight and track tortuosity and their respective relationships with collision risk for raptors may explain why white-tailed eagles generally had a higher collision risk than the other raptor species, as white-tailed eagles also spent more time in active flight and had less tortuous tracks compared to the other raptor species, with the exception of western osprey (Figure 3b,d,e). These differences in active flight and thereby collision risk may be linked to morphological differences between the raptor species. Peron [47] suggested that species with lower aspect ratios (ratio of wing span to chord) are more willing to use active flight i.e., more willing to leave thermals before reaching optimal height. Thus, possibly explaining why white-tailed eagles are more willing to utilize active flight compared to golden eagles, as white-tailed eagles also have a lower aspect ratio, i.e., white-tailed eagles have a larger wing area relative to their wing span [47]. Contrary to the expectation that birds that spent a large proportion of tracks looking down would result in an increased collision risk, this was not proven by the results in this case study. The univariate analysis indicated a negative relationship between risk proportion and time spent looking down for raptor tracks, i.e., time spent looking down did not increase collision risk. In the multivariate analysis for raptor tracks, head position was also weighed as an important predictor of collision risk (Figure 7b).

Moreover, no clear strong relationships were found in the univariate analysis between collision risk and the weather and temporal variables, respectively. However, for all raptor tracks and white-tailed eagle tracks there was a weak negative relationship between collision risk and temperature, and for all risk tracks, there was a positive, but weak, relationship between collision risk and time of day. Moreover, time of year, time of day, wind speed, and cloud coverage were important predictors of collision risk in the multivariate analysis for raptor tracks, where these four variables were included in six of the eight model terms with an evidence weight > 0.8 (Figure 7b). Furthermore, the multivariate analysis for all species tracks collectively indicated species to be the single most important predictor of collision risk. Thus, indicating that collision risk is species-specific, confirming the hypothesis that collision risk could be predicted by species.

4.2. Species-Specificity of Behavioral Traits

The behavioral traits head position and active flight appears to be species-specific (Figure 3c,d). Raptors generally spent more time looking down compared to the other study species, particularly, grey heron, great cormorant, common crane, and goose spp. (Figure 3c). These species generally did not spend any time looking down ($median = 0.00$). The differing foraging ecology between these species and the raptor species is a highly plausible reason for this finding, as all raptor species in this study, with the exception of western osprey, also foraged within the study site. These differences in foraging ecology are also conveyed by species differences in track tortuosity and symmetry, where raptors generally had more tortuous and asymmetric tracks (Figure 3a,b). Foraging ecology as a potential determining factor in regard to time spent looking down and track tortuosity and asymmetry is further supported by Linder et al. [28] who found a positive correlation between time spent looking down and track asymmetry and tortuosity, respectively, i.e., birds spending more time looking down also have more tortuous and asymmetric tracks. Thus, making it likely that these behavioral traits all being associated with the same determining factor, e.g., foraging ecology. Furthermore, head position, track tortuosity, and symmetry have also been linked to different flight strategies, as the utilization of soaring flight is associated with birds spending more time looking down and having asymmetric and tortuous tracks [28]. In this study, raptors generally spent little time in active flight, whereas, most other study species, e.g., grey heron, great cormorant, common crane, crow spp., and gull spp., spent more than 50% of frames engaging in active flight (Figure 3d). These differences in active flight can be linked to morphological differences between these species.

A phylogenetic signal was found for the flight behavioral traits, head position, active flight, and track symmetry, thus, confirming that these behavioral traits were correlated with phylogenetic relatedness. For track tortuosity the phylogenetic signal was weaker

than expected under Brownian motion ($K < 1$). Blomberg et al. [23] found that behavioral traits tend to show less phylogenetic signal than morphological traits. This is presumed to be due to the faster evolution rate of behavioral traits compared to morphological traits [23,48]. However, this was not the case in this study as three of the behavioral traits had *K*-values > 1, indicating that these behavioral traits are phylogenetically conserved i.e., close relatives had more similar flight behavior in regard to these traits than expected under Brownian motion [25]. More specifically, the *K*-value for active flight was the highest, which may be associated with the close relation between this behavioral trait and morphological traits e.g., wing loading and aspect ratio. Furthermore, a high phylogenetic signal was also found for the head position. This behavioral trait is presumably linked to the variation in foraging behaviors between the species and Weeks et al. [49] found foraging behavior to be significantly correlated with morphological traits, hence, a possible correlation between head position and morphological traits may explain the high phylogenetic signal. The phylogenetic signal was not as apparent for track symmetry and tortuosity, with both *K*-values ≈ 1. Similar to head position and active flight these two behavioral tracks are also associated with both foraging ecology and morphological traits. However, track symmetry and tortuosity are presumably more dependent on other factors, e.g., obstacle avoidance.

5. Conclusions

To our knowledge, this is the first study quantifying species-specific flight behavior in association with turbine collision risk. The findings of species-specific flight behavior were confirmed by a strong phylogenetic signal for the behavioral traits, head position, and active flight. Track tortuosity and track symmetry were also species-specific, but the phylogenetic signal was not stronger than expected under Brownian motion. All four behavioral traits were also shown to be important predictors of collision risk. The results of this study can be used to identify risk-prone species based on flight behavior and phylogenetic relatedness. The most important predictor of collision risk identified in this study was track tortuosity, with lower tortuosity increasing collision risk. Moreover, white-eagles were identified as a risk-prone species, based on their flight behavior and the high proportion of tracks in the risk zone. However, collision risk is also site-specific, and the results of the case study are, therefore, not directly applicable to site-specific conservation practices, but they can be used to give a general indication of risk-prone species. Thus, suggesting that white-tailed eagles are relevant to further investigate in site-specific contexts. It should be noted that these results are based on the proportion of time spent within 100 m proximity to the nearest turbine as a proxy for collision risk, more accurate results can only be achieved if it is possible to observe the behavior of individuals prior to actual collisions with wind turbines. It would take a large amount of time to collect such data collection due to the infrequency of collisions.

Author Contributions: Conceptualization, A.C.L., B.L., C.P., D.B. and H.L.; methodology, A.C.L., B.L., C.P., D.B. and H.L.; formal analysis, A.C.L.; investigation, A.C.L. and H.L.; resources, B.L.; data curation, A.C.L. and H.L.; writing—original draft preparation, A.C.L.; writing—review and editing, A.C.L., B.L., C.P. and D.B.; visualization, A.C.L.; supervision, B.L., C.P. and D.B. All authors have read and agreed to the published version of the manuscript.

Funding: This project was supported by Vattenfall and the Aalborg Zoo Conservation Foundation (AZCF: Grant number 09-2020).

Data Availability Statement: The data presented in this study are available on request from the corresponding author.

Acknowledgments: Thanks to Vattenfall for making data available and a special thanks to Tyler Derritt and the rest of the IdentiFlight team for technical assistance.

Conflicts of Interest: The authors declare no conflict of interest.

Appendix A. Study Site

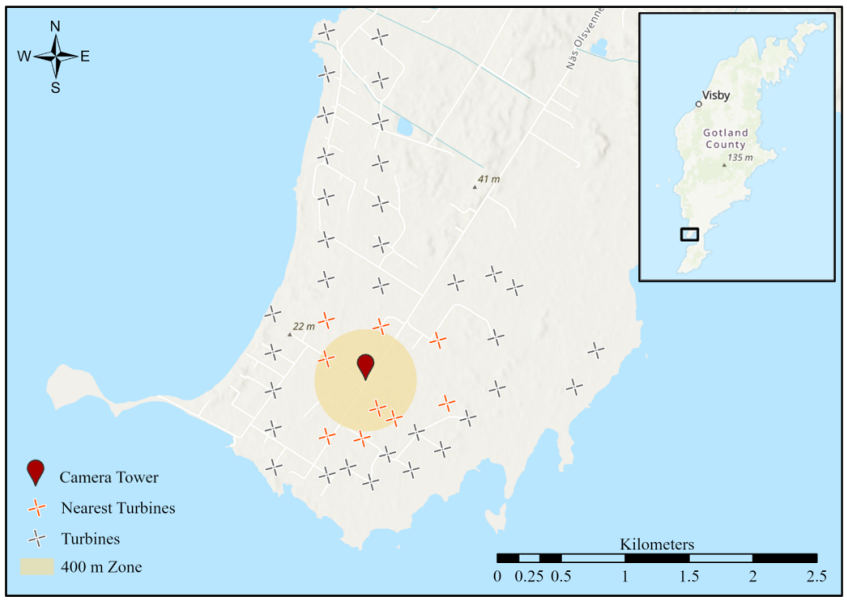

Figure A1. The IdentiFlight tower (red drop) and the observational area (orange circle), i.e., a 400 m zone around the tower. The nine wind turbines covered by the camera system (orange crosses) and other turbines (grey crosses) within the wind farm [28].

Appendix B. IdentiFlight System

Appendix B.1. IdentiFlight Camera System

Figure A2. Camera tower at study site.

Appendix B.2. Curtailment Prescription

For each turbine an outer and inner cylinder are predefined. If a bird that has been classified by the system as a protected species enters the inner cylinder a curtailment order is issued, resulting in the curtailment of the specific turbine. If the bird is present in the area between the outer and inner cylinder a curtailment order is only issue when certain criteria are met e.g., the bird is flying towards the particular turbine with a high flight speed (Table A1) [28].

Table A1. Turbine details in relation to curtailment for covered and partially covered wind turbines [28].

Model	Number of Turbines	Rotor Diameter (m)	Hub Height (m)	Radius Outer Cylinder (m)	Radius Inner Cylinder (m)	Height Outer Cylinder (m)	Height Inner Cylinder (m)
Covered							
Vestas V27	1	27	31	700	250	300	200
Vestas V29	1	29	31	700	250	300	200
Vestas V90	1	90	80	700	400	400	250
Partially covered							
Kenersys K100	1	100	85	600	300	400	250
Vestas V47	2	47	45	600	300	300	200
Vestas V90	2	90	80	700	300	400	250
Vestas V100	1	95	100	700	400	400	250

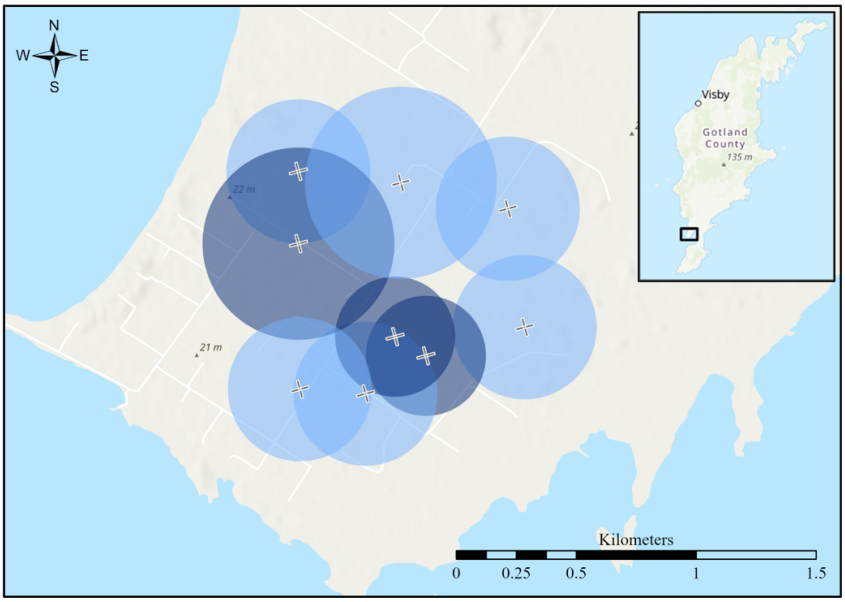

Figure A3. The radius of the inner cylinder for each turbine also indicating if the turbine is fully covered (dark blue) or partially covered (light blue) by the IdentiFlight camera tower.

Appendix C. Operational Days

Table A2. Number of days where the camera system was operational, number of days with observations of the selected bird species.

Year	Month	Operational Days	Days with Birds
2020	February	20	15
2020	March	31	31
2020	April	30	28
2020	May	31	28
2020	June	14	14
2020	July	15	15
2020	August	22	22
2020	September	30	27
2020	October	31	15
2020	November	30	13
2020	December	31	17
2021	January	31	20
2021	February	28	23
2021	March	31	28
	Total	155	145

Appendix D. Tracks

Table A3. Species and number of tracks for each species that are included in the analyses.

Species	Number of Tracks
Golden eagle	85
White-tailed eagle	178
Red kite	42
Black kite	16
Common buzzard	85
Western osprey	6
Grey heron	135
Great cormorant	83
Common crane	18
Goose spp.	28
Crow spp.	97
Gull spp.	114
Total	887

Appendix E. Calculations of Track Tortuosity and Symmetry

Appendix E.1. Track Tortuosity

Track tortuosity was calculated for each track using Equation (A1) (Figure A4) [28]. This resulted in a measure of deviations from the shortest flight path, where a value of 1 indicates a completely straight flight path, i.e., a low tortuosity. The lower the ratio the more tortuous the flight path [28].

$$Track\ tortuosity = \frac{Direct\ track\ length}{Actual\ track\ length} \quad \text{(A1)}$$

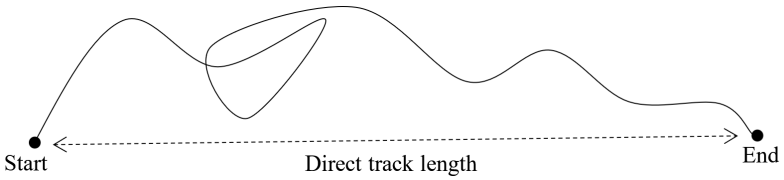

Figure A4. Portrayal of a track, showing direct track length (the dotted arrow) in comparison to actual track length [28].

Appendix E.2. Track Symmetry

An individuals track consists of multiple points connected in a chronological order [28]. Each turn an individual makes can therefore be described by the angle between the connected points. The track angles ranged from $-180°$ to $180°$, thus, distinguishing between left and right turns (Figure A5) [28].

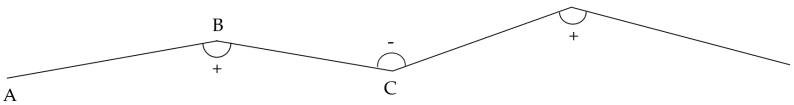

Figure A5. Track model in which right turns ranged from 0 to $180°$ and left turns from $-180°$ to 0 [28].

The angles of each track were calculated using the inverse trigonometric function of cosine (arccos) (Equation (A2)) [28]. A, B and C represent track points, where AB is the distance from point A to point B, and BC is the distance between point B and C, etc. (Figure A5).

$$\angle B = arccos\left(\frac{AB^2 + BC^2 - AC^2}{2 \cdot AB \cdot BC}\right) \quad \text{(A2)}$$

Equation (A3) was used to calculate the track symmetry for each track, where a value of 0 represents a perfectly symmetrical track. Hence, the larger the value the more asymmetrical the track [28].

$$Tracksymmetry = \left| \sum_{i=1}^{n} \angle_i \right| \tag{A3}$$

Appendix F. Risk Zones

Table A4. Model type, number of turbines, rotor diameter and the radius of risk zone around each turbine.

Model	Number of Turbines	Radius of Rotor (m)	Radius of Risk Zone (m)
Covered			
Vestas V27	1	13.5	113.5
Vestas V29	1	14.5	114.5
Vestas V90	1	45	145
Partially covered			
Kenersys 2500 100	1	50	150
Vestas V47	2	23.5	123.5
Vestas V90	2	22.5	122.5
Vestas V100	1	47.5	147.5

Appendix G. Data Exploration

Appendix G.1. Variance Inflation Factor Analysis

A variance inflation factor (VIF) analysis was used to assess the collinearity of the explanatory variables. A backward selection was used, removing the variable with the highest VIF value and recalculating the VIF values for the remaining variables after each iteration, until all VIF values were smaller than 2 [50].

Table A5. Variance inflation factor (VIF) values for the explanatory variables.

Covariate	All Tracks	Raptor Tracks	All Risk Tracks	Raptor Risk Tracks
		Initial VIF values (iteration 1)		
Head position	1.42	1.23	1.52	1.39
Active flight	1.34	1.17	1.44	1.26
Track symmetry	1.50	1.51	1.64	1.57
Track tortuosity	1.64	1.56	1.82	1.83
Cloud coverage	1.18	1.21	1.22	1.41
Temperature	1.52	1.64	1.45	9.75
Wind speed	1.10	1.13	1.09	1.44
Time of year	1.49	1.54	1.50	9.08
Time of day	1.04	1.06	1.07	1.23

Appendix G.2. Spearman's Correlation Coefficient and Pairwise Scatter-Plots

To assess collinearity Spearman's correlation coefficient was calculated among the covariates and pairwise scatter-plots were created to detect obvious correlations among the covariates.

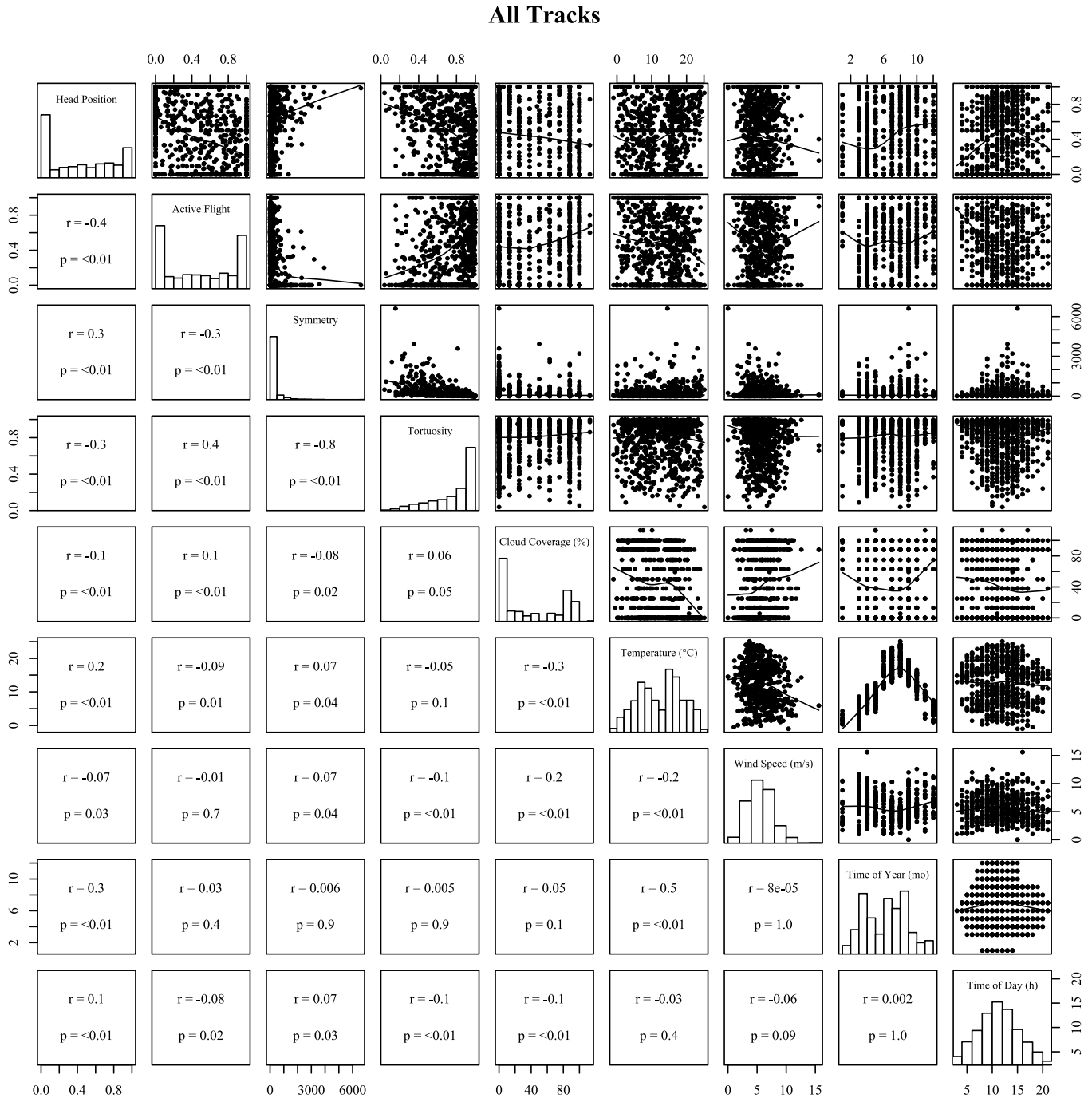

Figure A6. Correlation between the different continuous predictor variables for all tracks.

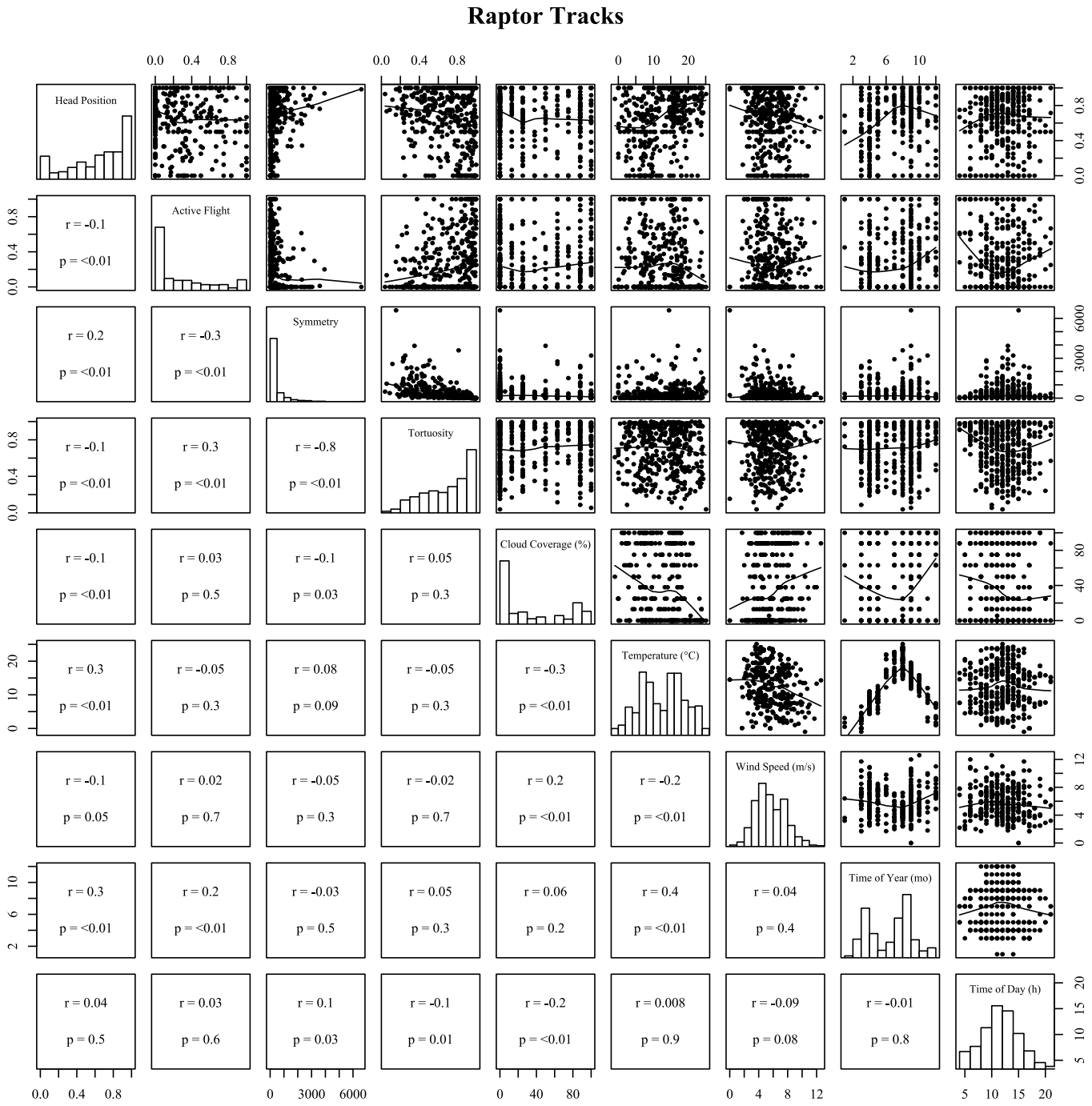

Figure A7. Correlation between the different continuous predictor variables for raptor tracks.

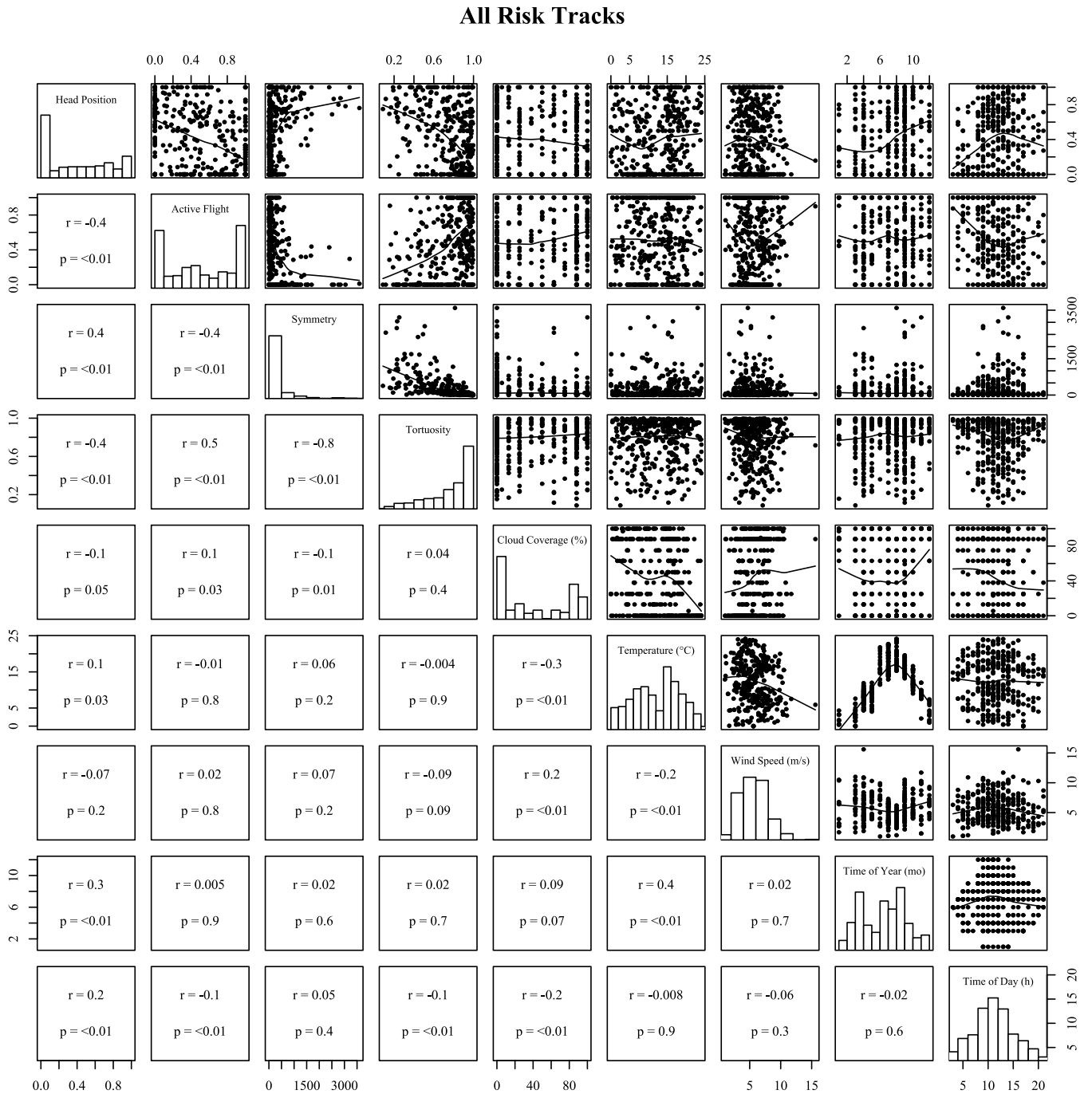

Figure A8. Correlation between the different continuous predictor variables for all risk tracks.

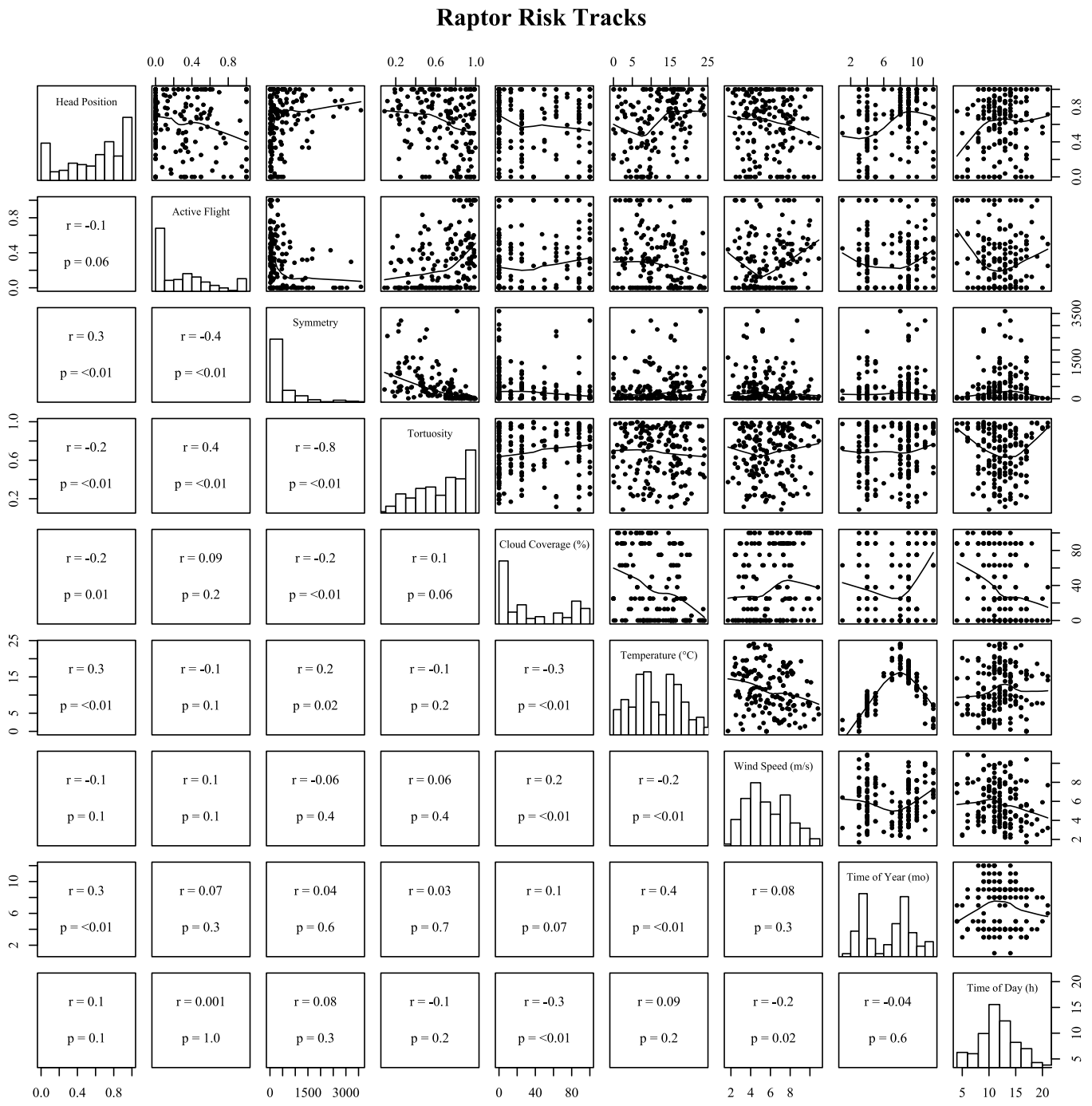

Figure A9. Correlation between the different continuous predictor variables for raptor risk tracks.

Appendix H. Univariate Results

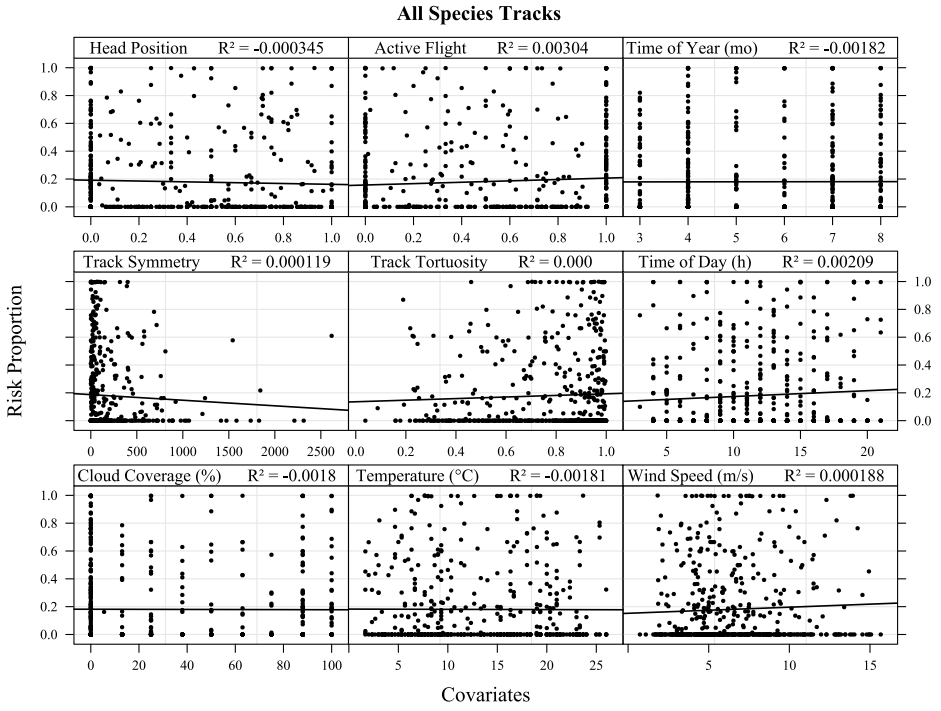

Figure A10. Proportion time spent in risk zone as a function of each possible explanatory variable for all tracks. A regression trend line is depicted for each plot along with the coefficient of determination (R^2) and significance level.

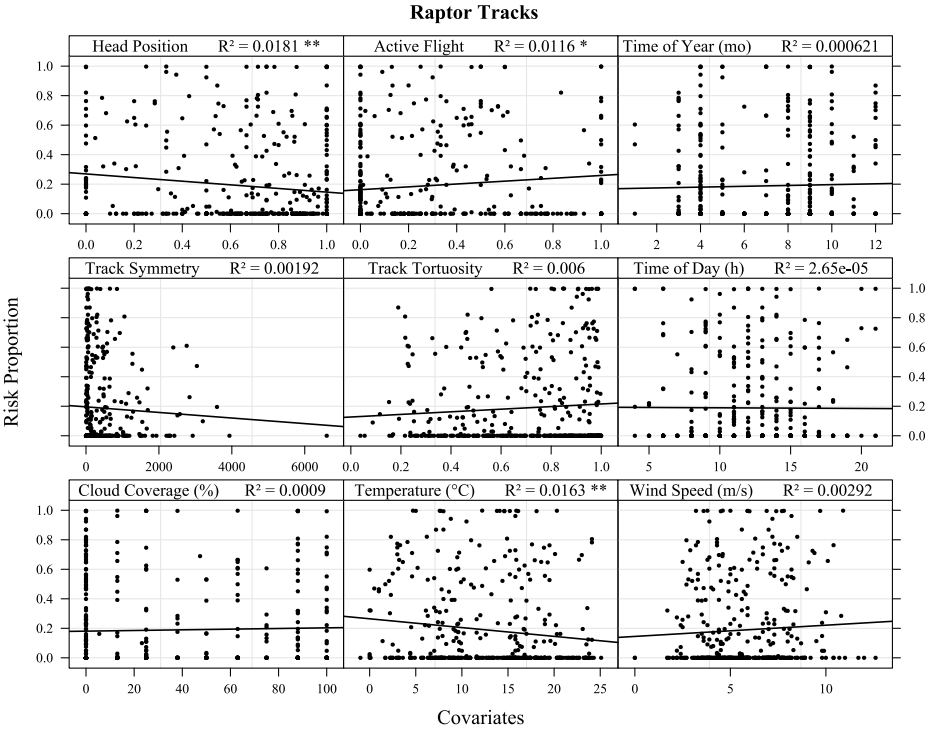

Figure A11. Proportion time spent in risk zone as a function of each possible explanatory variable for all raptor tracks. A regression trend line is depicted for each plot along with the coefficient of determination (R^2) and significance level (* $p < 0.05$, ** $p < 0.01$).

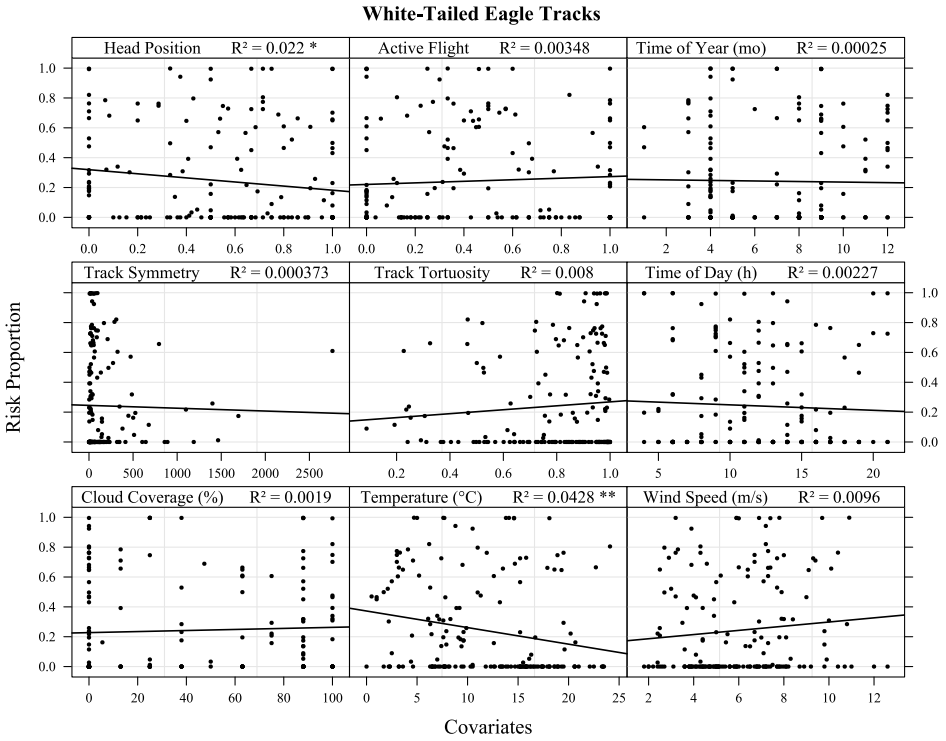

Figure A12. Proportion time spent in risk zone as a function of each possible explanatory variable for all white-tailed eagle tracks. A regression trend line is depicted for each plot along with the coefficient of determination (R^2) and significance level (* $p < 0.05$, ** $p < 0.01$).

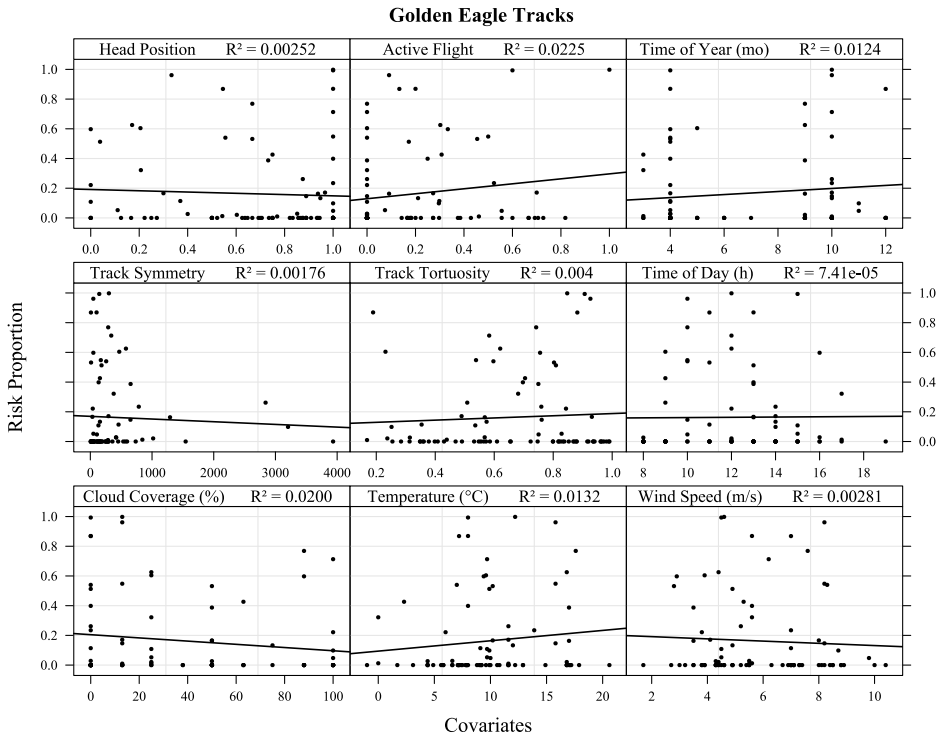

Figure A13. Proportion time spent in risk zone as a function of each possible explanatory variable for all golden eagle tracks. A regression trend line is depicted for each plot along with the coefficient of determination (R^2) and significance level.

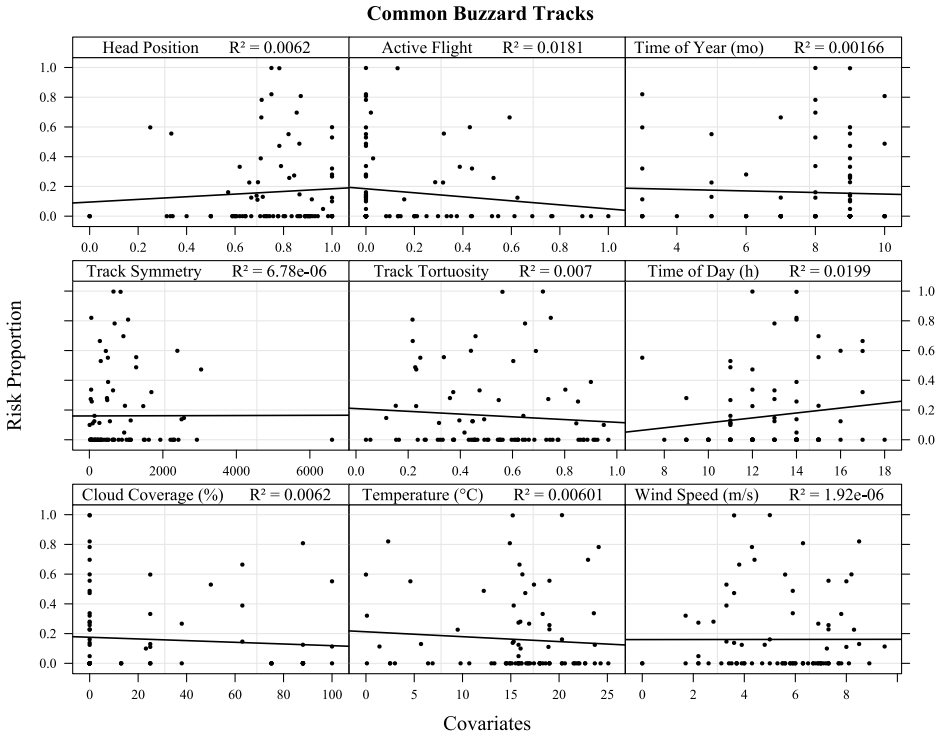

Figure A14. Proportion time spent in risk zone as a function of each possible explanatory variable for all common buzzard tracks. A regression trend line is depicted for each plot along with the coefficient of determination (R^2) and significance level.

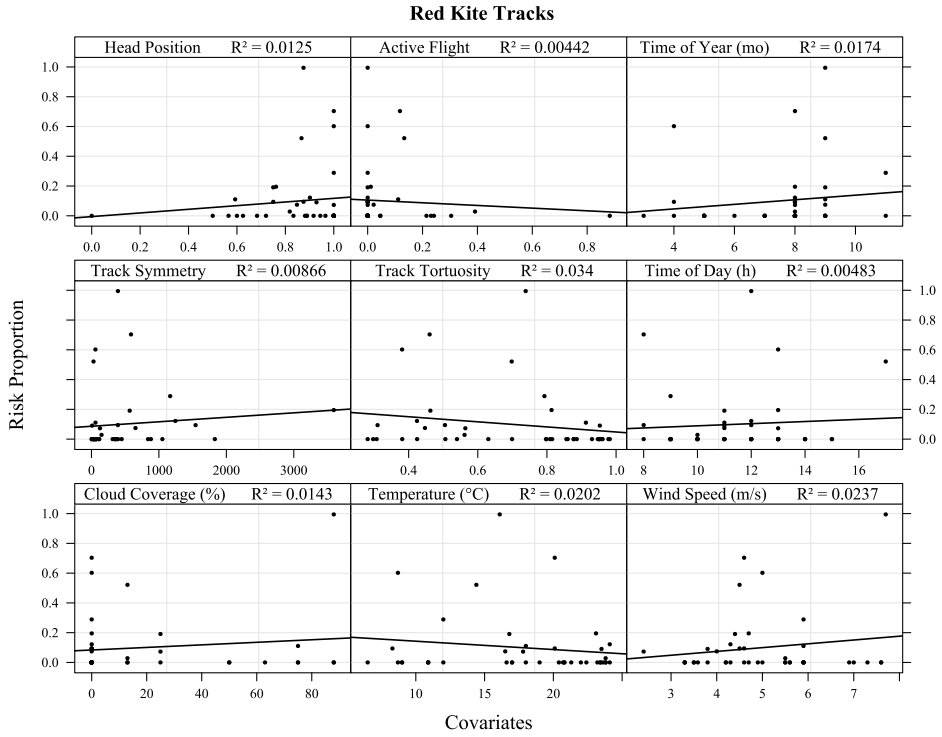

Figure A15. Proportion time spent in risk zone as a function of each possible explanatory variable for all red kite tracks. A regression trend line is depicted for each plot along with the coefficient of determination (R^2) and significance level.

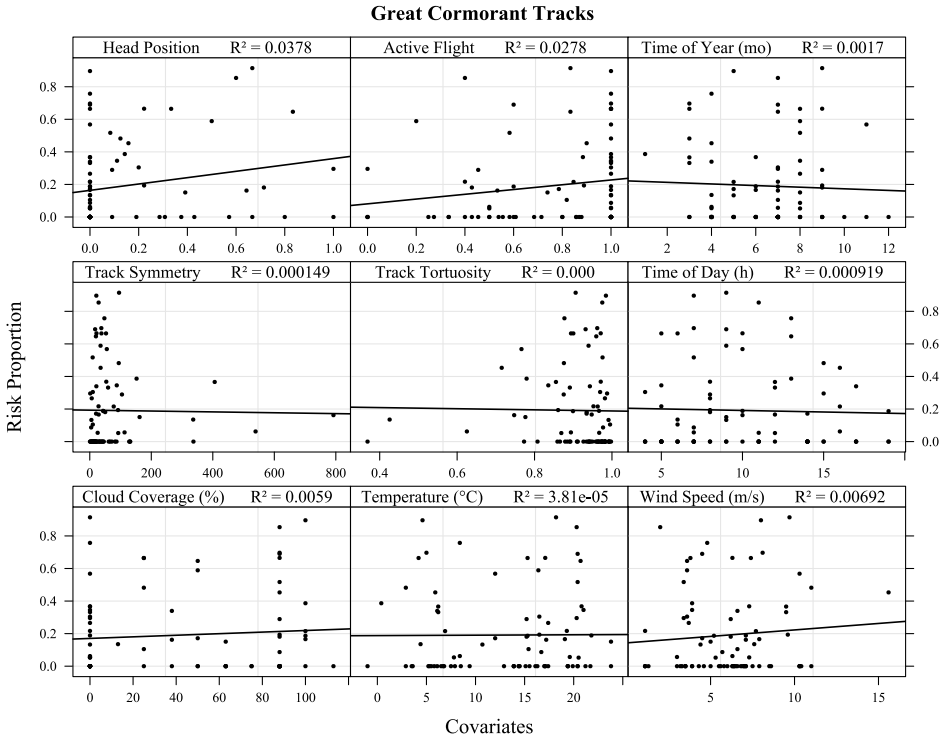

Figure A16. Proportion time spent in risk zone as a function of each possible explanatory variable for all great cormorant tracks. A regression trend line is depicted for each plot along with the coefficient of determination (R^2) and significance level.

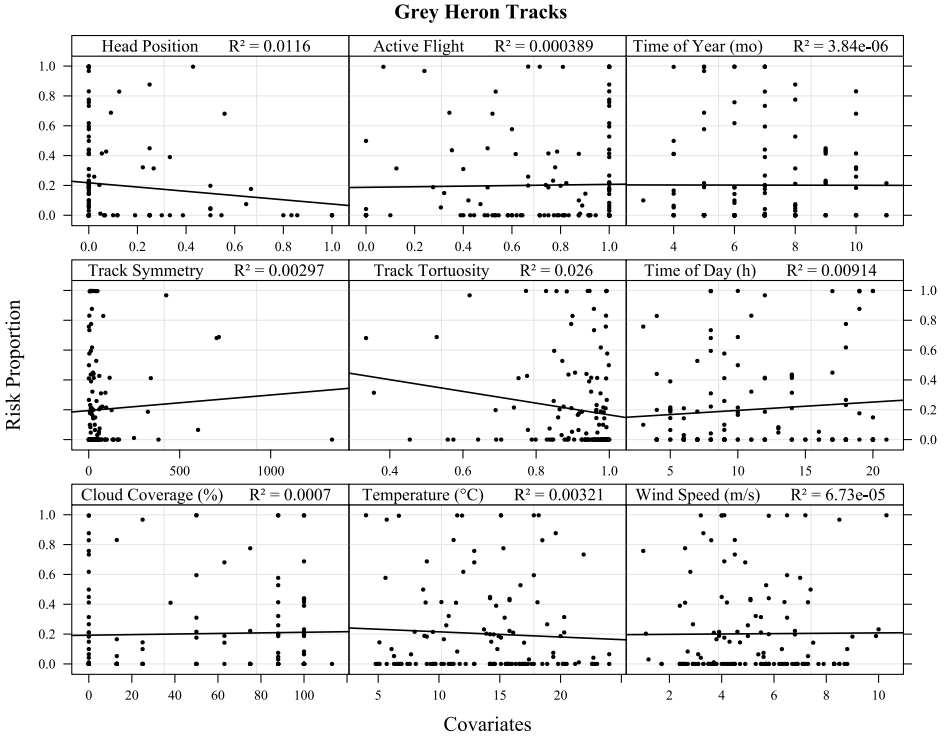

Figure A17. Proportion time spent in risk zone as a function of each possible explanatory variable for all grey heron tracks. A regression trend line is depicted for each plot along with the coefficient of determination (R^2) and significance level.

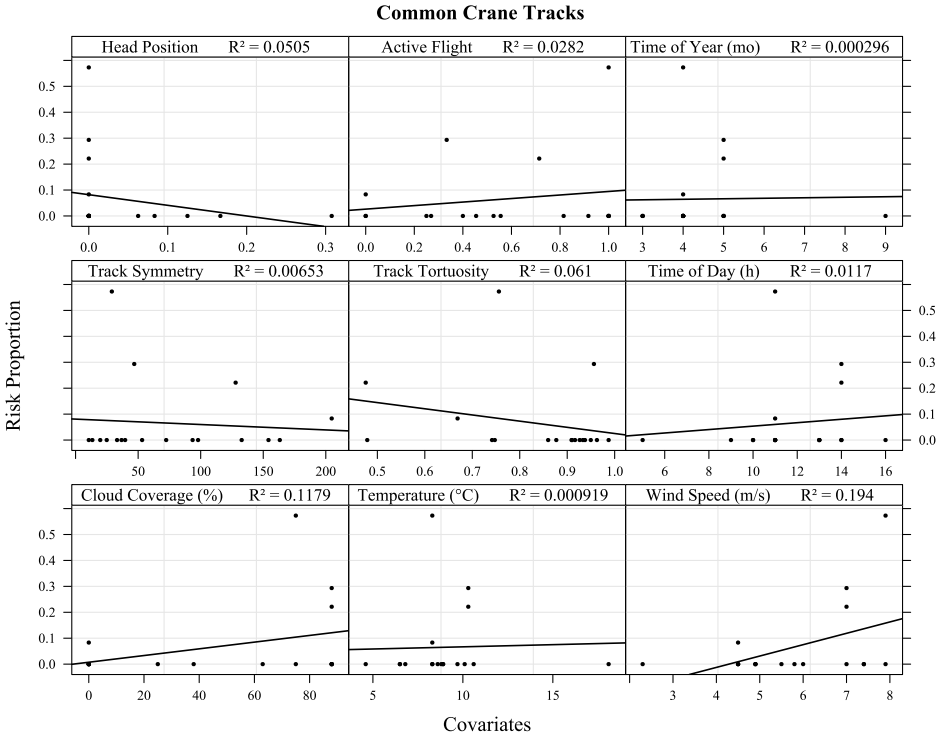

Figure A18. Proportion time spent in risk zone as a function of each possible explanatory variable for all common crane tracks. A regression trend line is depicted for each plot along with the coefficient of determination (R^2) and significance level.

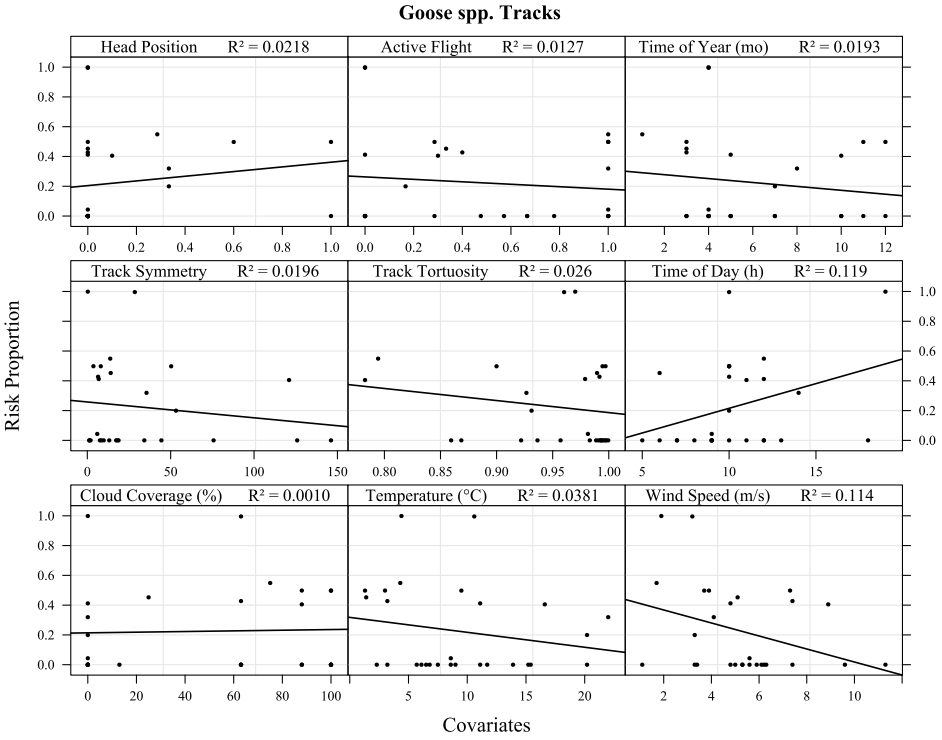

Figure A19. Proportion time spent in risk zone as a function of each possible explanatory variable for all goose spp. tracks. A regression trend line is depicted for each plot along with the coefficient of determination (R^2) and significance level.

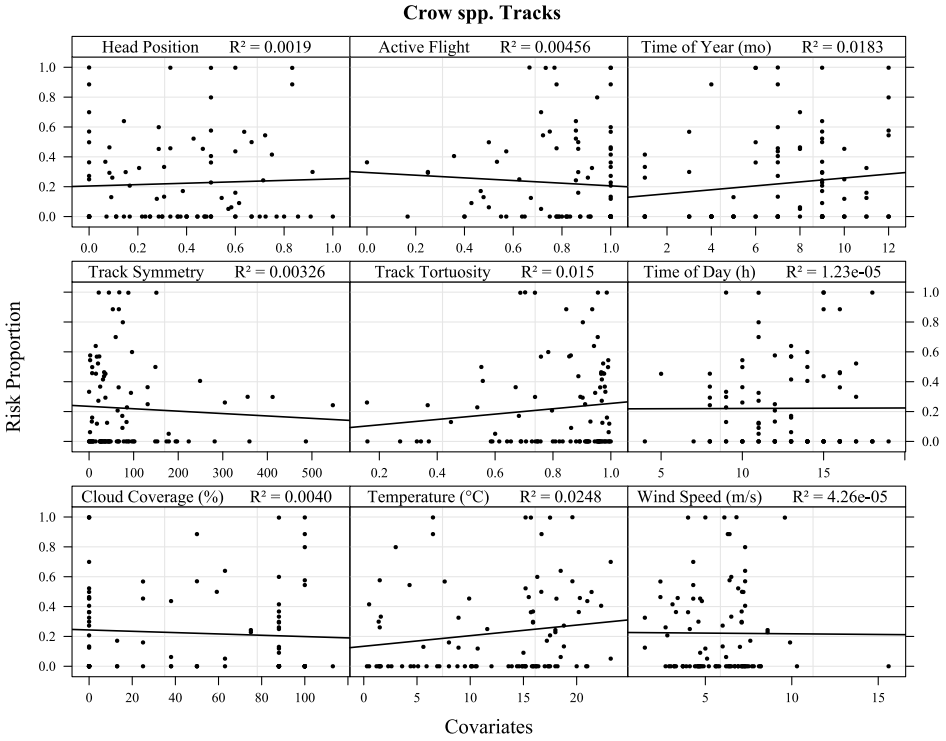

Figure A20. Proportion time spent in risk zone as a function of each possible explanatory variable for all crow spp. tracks. A regression trend line is depicted for each plot along with the coefficient of determination (R^2) and significance level.

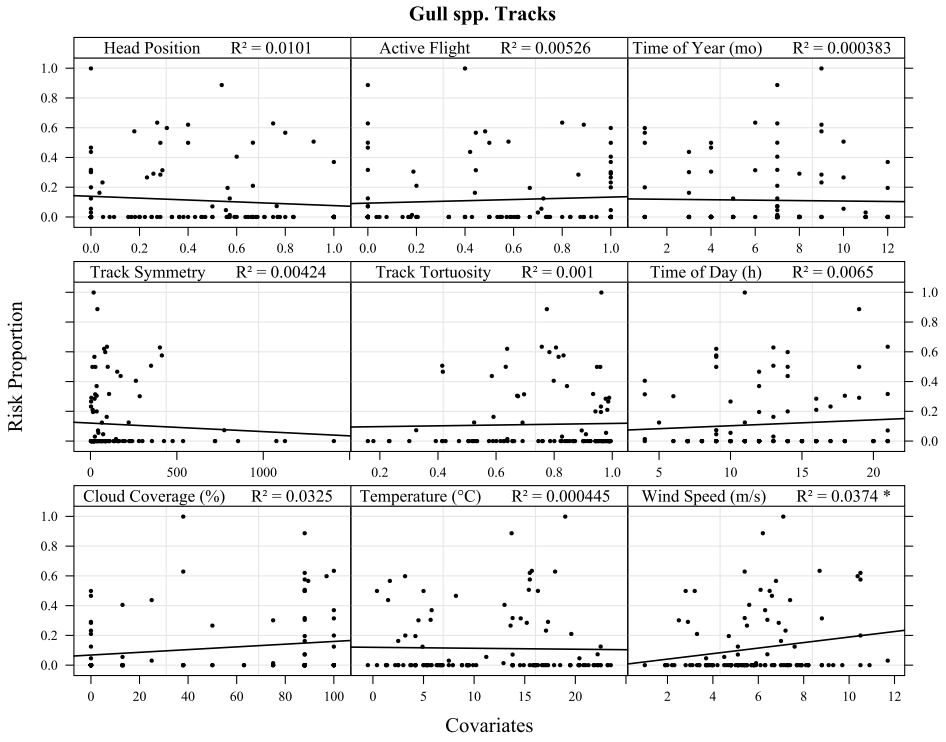

Figure A21. Proportion time spent in risk zone as a function of each possible explanatory variable for all gull spp. tracks. A regression trend line is depicted for each plot along with the coefficient of determination (R^2) and significance level (* $p < 0.05$).

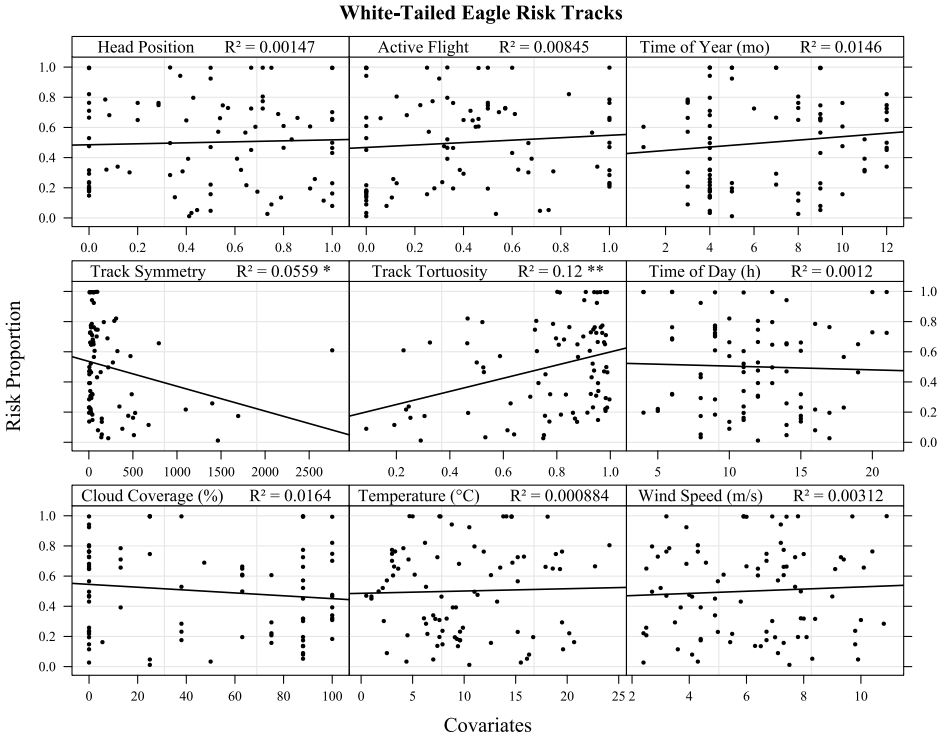

Figure A22. Proportion time spent in risk zone as a function of each possible explanatory variable for white-tailed eagle risk tracks. A regression trend line is depicted for each plot along with the coefficient of determination (R^2) and significance level (* $p < 0.05$, ** $p < 0.01$).

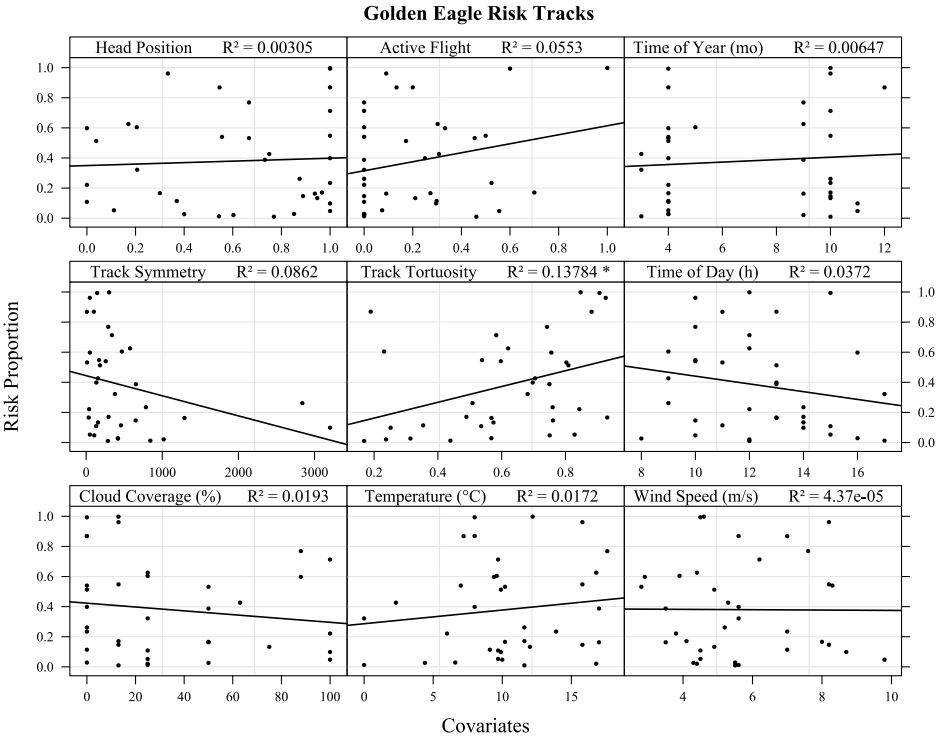

Figure A23. Proportion time spent in risk zone as a function of each possible explanatory variable for golden eagle risk tracks. A regression trend line is depicted for each plot along with the coefficient of determination (R^2) and significance level (* $p < 0.05$).

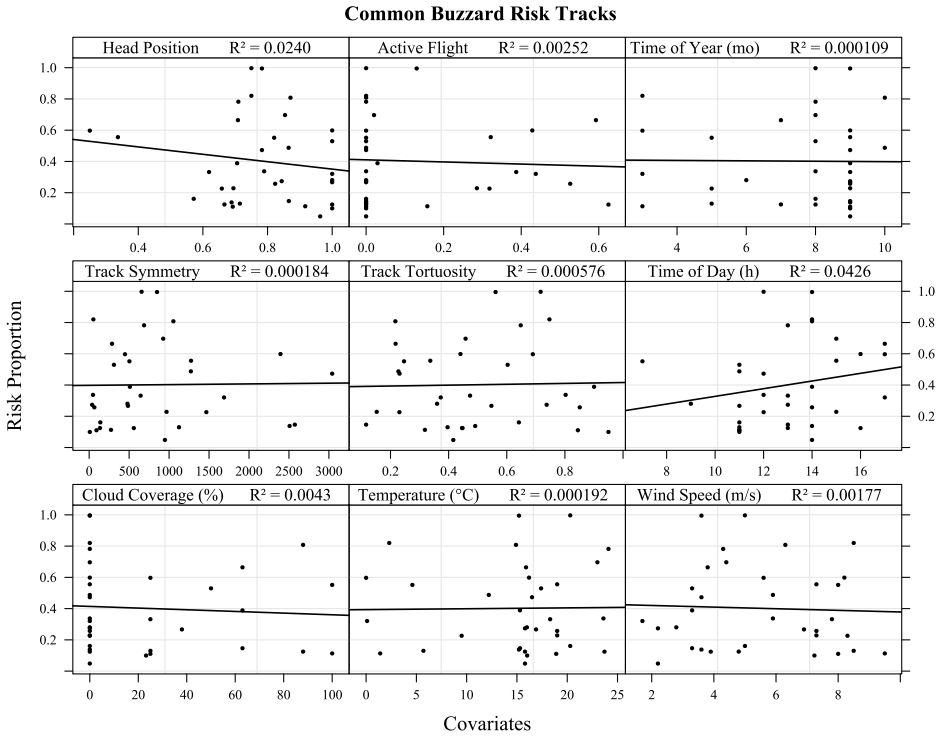

Figure A24. Proportion time spent in risk zone as a function of each possible explanatory variable for common buzzard risk tracks. A regression trend line is depicted for each plot along with the coefficient of determination (R^2) and significance level.

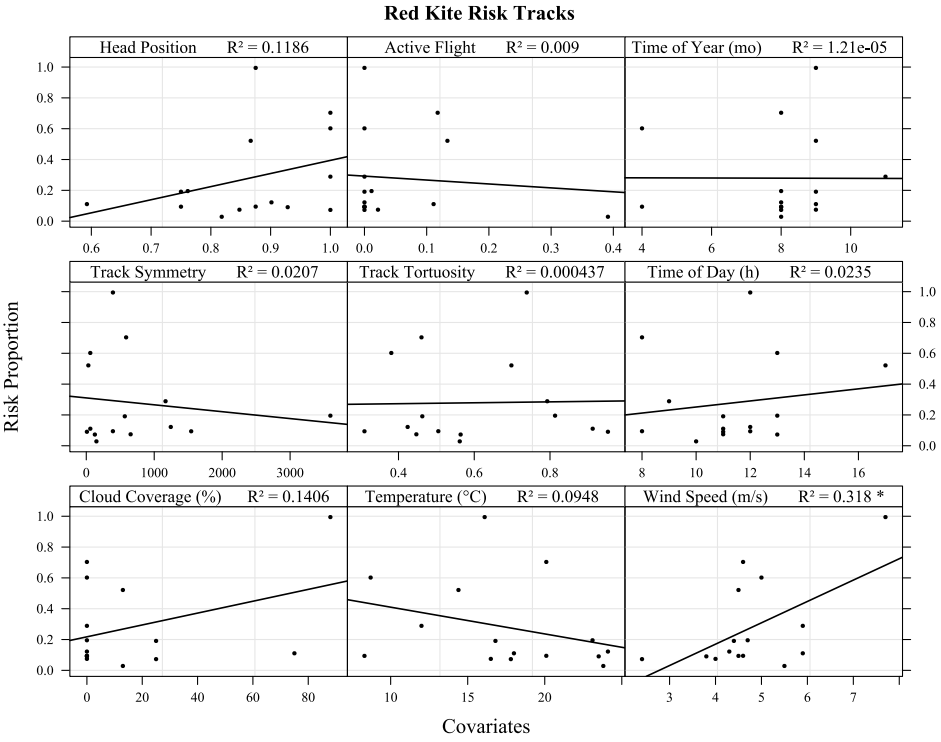

Figure A25. Proportion time spent in risk zone as a function of each possible explanatory variable for red kite risk tracks. A regression trend line is depicted for each plot along with the coefficient of determination (R^2) and significance level (* $p < 0.05$).

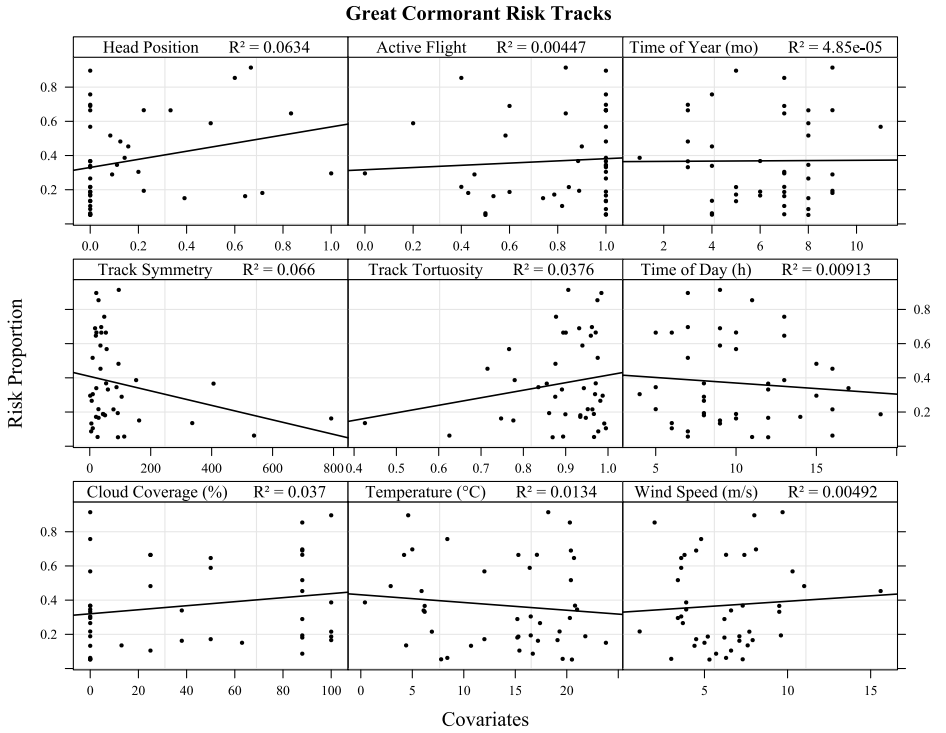

Figure A26. Proportion time spent in risk zone as a function of each possible explanatory variable for great cormorant risk tracks. A regression trend line is depicted for each plot along with the coefficient of determination (R^2) and significance level.

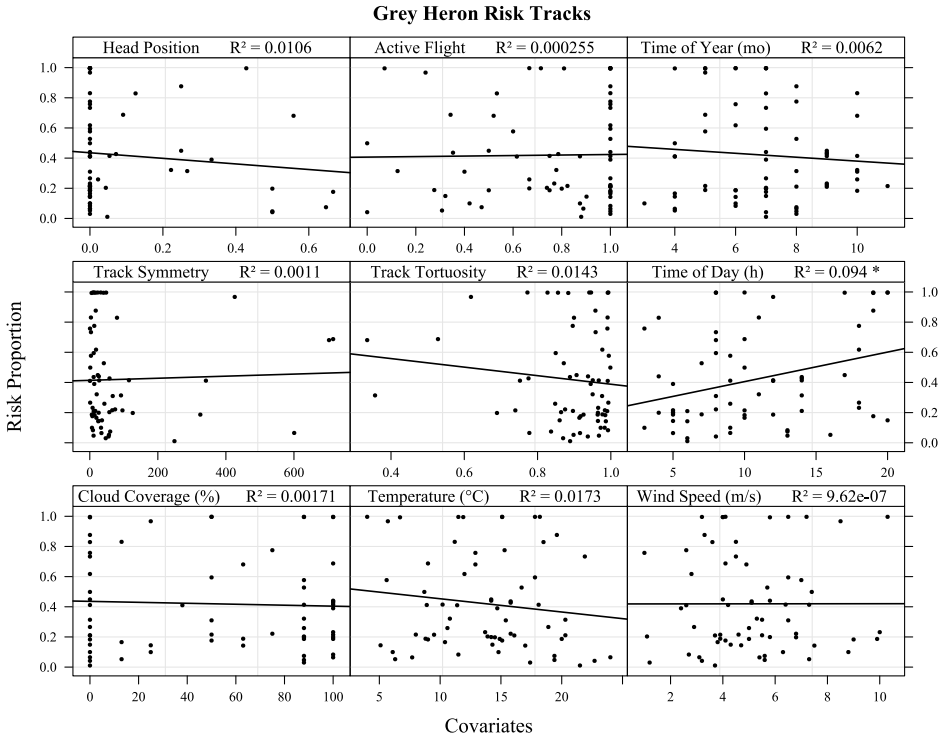

Figure A27. Proportion time spent in risk zone as a function of each possible explanatory variable. for grey heron risk tracks. A regression trend line is depicted for each plot along with the coefficient of determination (R^2) and significance level (* $p < 0.05$).

Appendix I. Model Selection

The automated model selection was carried out for models both with and without interactions for all tracks, raptor tracks, all risk tracks, and raptor risk tracks. For each subset the models with and without interactions were compared based on their respective AIC values. Moreover, an Anova test using the χ^2 test statistic was also used to assess the goodness of fit of the nested regression models, i.e., the models with and without interactions [39]. The model with interactions was selected as the best model if the addition of interaction terms significantly increased the model's goodness of fit, if not the simpler of the two models, i.e., the model without interactions, was selected. The models that were not selected as the best models are presented below.

Table A6. Details of the automated model selection completed with *glmulti*. The * annotation indicates that the addition of interaction terms significantly improved the model's goodness of fit.

Name	No. of Tracks	No. of Generations	Best AIC
All tracks			
Without interactions	886	250	274
With interactions	886	640	274
Raptor tracks *			
Without interactions	411	250	155
With interactions	411	550	153
All risk track			
Without interactions	387	250	130
With interactions	387	690	128
Raptor risk tracks			
Without interactions	178	250	65.7
With interactions	178	460	61.7

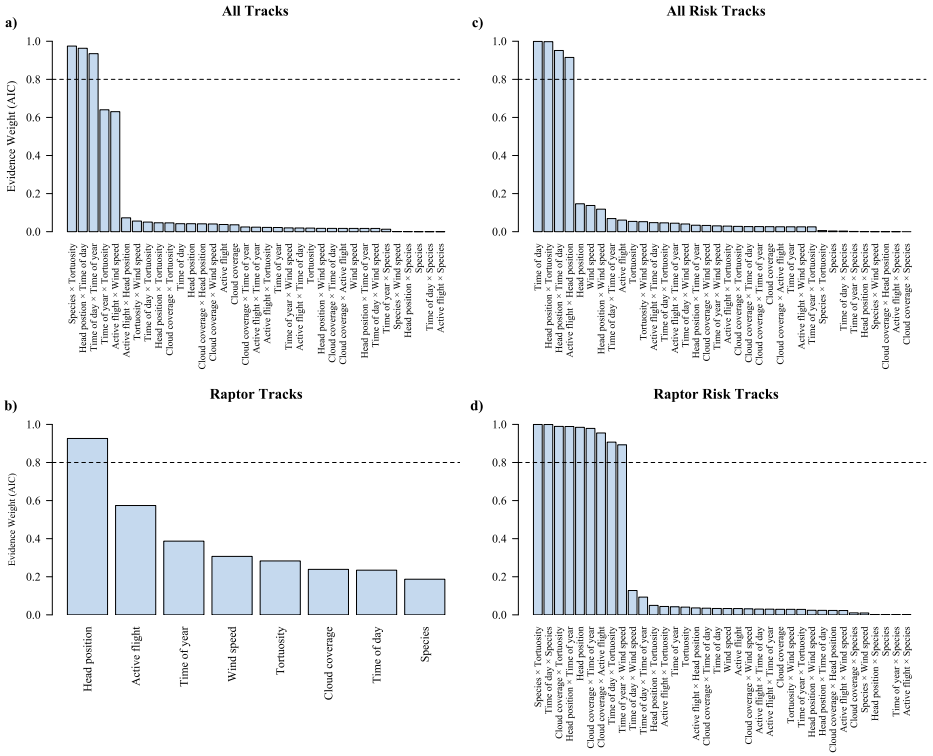

Figure A28. Each term's estimated importance computed as the sum of the relative weights of all models in which the term appears.

References

1. Drewitt, A.L.; Langston, R.H.W. Assessing the Impacts of Wind Farms on Birds. *IBIS* **2006**, *148*, 29–42. [CrossRef]
2. Madders, M.; Whitfield, D.P. Upland Raptors and the Assessment of Wind Farm Impacts. *IBIS* **2006**, *148*, 43–56. [CrossRef]
3. de Lucas, M.; Janss, G.F.E.; Whitfield, D.P.; Ferrer, M. Collision Fatality of Raptors in Wind Farms does not Depend on Raptor Abundance. *J. Appl. Ecol.* **2008**, *45*, 1695–1703. [CrossRef]
4. Smallwood, K.S.; Thelander, C. Bird Mortality in the Altamont Pass Wind Resource Area, California. *J. Wildl. Manag.* **2008**, *72*, 215–223. [CrossRef]
5. Bevanger, K.; Berntsen, F.; Clausen, S.; Dahl, E.L.; Flagstad, Ø.; Follestad, A.; Halley, D.; Hanssen, F.; Johnsen, L.; Kvaløy, P.; et al. *Pre- and Post-Construction Studies of Conflicts between Birds and Wind Turbines in Coastal Norway (Bird-Wind). Report on Findings 2007–2010*; Norsk Institutt for Naturforskning: Trondheim, Norway, 2010.
6. Katzner, T.E.; Brandes, D.; Miller, T.; Lanzone, M.; Maisonneuve, C.; Tremblay, J.A.; Mulvihill, R.; Merovich, G.T., Jr. Topography Drives Migratory Flight Altitude of Golden Eagles: Implications for On-Shore Wind Energy Development. *J. Appl. Ecol.* **2012**, *49*, 1178–1186. [CrossRef]
7. Loss, S.R.; Will, T.; Marra, P.P. Estimates of Bird Collision Mortality at Wind Facilities in the Contiguous United States. *Biol. Conserv.* **2013**, *168*, 201–209. [CrossRef]
8. Marques, A.T.; Batalha, H.; Rodrigues, S.; Costa, H.; Pereira, M.J.R.; Fonseca, C.; Mascarenhas, M.; Bernardino, J. Understanding Bird Collisions at Wind Farms: An Updated Review on the Causes and Possible Mitigation Strategies. *Biol. Conserv.* **2014**, *179*, 40–52. [CrossRef]
9. Watson, R.T.; Kolar, P.S.; Ferrer, M.; Nygård, T.; Johnston, N.; Hunt, W.G.; Smit-Robinson, H.A.; Farmer, C.J.; Huso, M.; Katzner, T.E. Raptor Interactions with Wind Energy: Case Studies from Around the World. *J. Raptor Res.* **2018**, *52*, 1–18. [CrossRef]
10. Perold, V.; Ralston-Paton, S.; Ryan, P. On a Collision Course? The Large Diversity of Birds Killed by Wind Turbines in South Africa. *J. Afr. Ornithol.* **2020**, *91*, 228–239. [CrossRef]
11. Powlesland, R.G. Impacts of Wind Farms on Birds: A Review. *Sci. Conserv.* **2009**, *289*, 51.
12. Barrios, L.; Rodríguez, A. Behavioural and Environmental Correlates of Soaring-bird Mortality at On-shore Wind Turbines. *J. Appl. Ecol.* **2004**, *41*, 72–81. [CrossRef]
13. Martin, G.R.; Portugal, S.J.; Murn, C.P. Visual Fields, Foraging and Collision Vulnerability in *Gyps* Vultures. *IBIS* **2012**, *154*, 626–631. [CrossRef]
14. Potier, S.; Duriez, O.; Cunningham, G.B.; Bonhomme, V.; O'Rourke, C.; Fernàndez-Juricic, E.; Bonadonna, F. Visual Field Shape and Foraging Ecology in Diurnal Raptors. *J. Exp. Biol.* **2018**, *221*, jeb177295. [CrossRef]
15. Janss, G. Avian mortality from power lines: A morphologic approach of a species-specific mortality. *Mol. Biol. Evol.* **2000**, *10*, 512–526. [CrossRef]
16. Therkildsen, O.R.; Elmeros, M.; Kahlert, J.; Desholm, M. *Baseline Investigations of Bats and Birds at Wind Turbine Test Centre Østerild*; Scientific Report from DCE—Danish Centre for Environment and Energy, No. 28; DCE: Aarhus, Denmark, 2012.
17. Navarrete, L.; Griffis-Kyle, K.L. Sandhill Crane Collisions with Wind Turbines in Texas. *Proc. N. Am. Crane Workshop* **2016**, *13*, 380.
18. Powlesland, R.G. *Bird Species of Concern at Wind Farms in New Zealand*; DOC Research & Development Series 317; Department of Conservation: Wellington, New Zealand, 2009.
19. Johnston, N.N.; Bradley, J.E.; Otter, K.A. Increased Flight Altitudes Among Migrating Golden Eagles Suggest Turbine Avoidance at a Rocky Mountain Wind Installation. *PLoS ONE* **2014**, *9*, e93030. [CrossRef] [PubMed]
20. Murgatroyd, M.; Photopoulou, T.; Underhill, L.G.; Bouten, W.; Amar, A. Where Eagles Soar: Fine-Resolution Tracking Reveals the Spatiotemporal Use of Differential Soaring Modes in a Large Raptor. *Ecol. Evol.* **2018**, *8*, 6788–6799. [CrossRef]
21. Marques, A.T.; Santos, C.D.; Hanssen, F.; Muñoz, A.; Onrubia, A.; Wikelski, M.; Moreira, F.; Palmeirim, J.M.; Silva, J.P. Wind Turbines Cause Functional Habitat Loss for Migratory Soaring Birds. *J. Anim. Ecol.* **2019**, *89*, 93–103. [CrossRef] [PubMed]
22. May, R.; Hoel, P.L.; Langston, R.; Dahl, E.L.; Bevanger, K.; Reitan, O.; Nygård, T.; Pedersen, H.C.; Røskaft, E.; Stokke, B.G. *Collision Risk in White-Tailed Eagles. Modelling Collision Risk Using Vantage Point Observations in Smøla Wind-Power Plant*; Norsk Institutt for Naturforskning: Trondheim, Norway, 2010.
23. Blomberg, S.P.; Garland, T., Jr.; Ives, A.R. Testing for Phylogenetic Signal in Comparative Data: Behavioral Traits are More Labile. *Evolution* **2003**, *57*, 717–745. [CrossRef]
24. Losos, J.B. Phylogenetic Niche Conservatism, Phylogenetic Signal and the Relationship Between Phylogenetic Relatedness and Ecological Similarity Among Species. *Ecol. Lett.* **2008**, *11*, 995–1003. [CrossRef]
25. Kamilar, J.M.; Cooper, N. Phylogenetic Signal in Primate Behaviour, Ecology and Life History. *Philos. Trans. R. Soc. B* **2013**, *368*, 20120341. [CrossRef] [PubMed]
26. Blomberg, S.P.; Garland, T., Jr. Tempo and Mode in Evolution: Phylogenetic Inertia, Adaptation and Comparative Methods. *J. Evol. Biol.* **2002**, *15*, 889–910. [CrossRef]
27. Herrera-Alsina, L.; Villegas-Patraca, R.; Eguiarte, L.E.; Artia, H.T. Bird communities and wind farms: A phylogenetic and morphological approach. *Biodivers. Conserv.* **2013**, *22*, 2821–2836. [CrossRef]
28. Linder, A.; Lyhne, H.; Laubek, B.; Bruhn, D.; Pertoldi, C. Quantifying Raptors' Flight Behavior to Assess Collision Risk and Avoidance Behavior to Wind Turbines. *submitted*.

29. McClure, C.J.W.; Martinson, L.; Allison, T.D. Automated Monitoring for Birds in Flight: Proof of Concept with Eagles at a Wind Power Facility. *Biol. Conserv.* **2018**, *224*, 26–33. [CrossRef]
30. McClure, C.J.W.; Rolek, B.W.; Dunn, L.; McCabe, J.D.; Martinson, L.; Katzner, T. Eagle Fatalities are Reduced by Automated Curtailment of Wind Turbines. *J. Appl. Ecol.* **2021**, *58*, 446–452. [CrossRef]
31. Esri; HERE; Garmin; FAO; NOAA; USGS. World Topographic Map. 2020. Available online: http://www.esri.com/ (accessed on 1 March 2021).
32. Wirdheim, A.; Corell, M. *Fågelrapport 2015*; Fågelåret 2015; BirdLife Sverige: Mörbylånga, Sweden, 2015.
33. Aldén, L.; Ottvall, R.; Soares, J.P.D.S.; Klein, J.; Liljenfeldt, J. *Rapport: Samexistens Örnar och Vindkraft på Gotland*; Uppsala Universitet: Visby, Sweden, 2017.
34. Esri. *ArcGIS Pro 2.5.0*; Environmental Systems Research Institute: Redlands, CA, USA, 2020.
35. SMHI, Swedish Meteorological and Hydrological Institute. 2020. Available online: www.smhi.se (accessed on 30 August 2022).
36. R Core Team. *R Version 4.0.3*; R Foundation for Statistical Computing: Vienna, Austria, 2020.
37. Zuur, A.F.; Ieno, E.N.; Elphick, C.S. A Protocol for Data Exploration to Avoid Common Statistical Problems. *Methods Ecol. Evol.* **2010**, *1*, 3–14. [CrossRef]
38. Calcagno, V.; de Mazancourt, C. glmulti: An R Package for Easy Automated Model Selection with (Generalized) Linear Models. *J. Stat. Softw.* **2010**, *34*, 1–29. [CrossRef]
39. Zuur, A.F.; Ieno, E.N.; Walker, N.J.; Saveliev, A.A.; Smith, G.M. *Mixed Effects Models and Extensions in Ecology with R*; Statistics for Biology and Health; Springer: New York, NY, USA, 2009.
40. Kumar, S.; Stecher, G.; Li, M.; Knyaz, C.; Tamura, K. MEGA X: Molecular Evolutionary Genetics Analysis across Computing Platforms. *Mol. Biol. Evol.* **2018**, *35*, 1547–1549. [CrossRef] [PubMed]
41. Tamura, K.; Nei, M. Estimation of the Number of Nucleotide Substitutions in the Control Region of Mitochondrial DNA in Humans and Chimpanzees. *Mol. Biol. Evol.* **1993**, *10*, 512–526. [PubMed]
42. Hillis, D.M.; Bull, J.J. An Empirical Test of Bootstrapping as a Method for Assessing Confidence in Phylogenetic Analysis. *Syst. Biol.* **1993**, *42*, 182–192. [CrossRef]
43. Pacheco, M.A.; Battistuzzi, F.U.; Lentino, M.; Aguilar, R.F.; Kumar, S.; Escalante, A.A. Evolution of Modern Birds Revealed by Mitogenomics: Timing the Radiation and Origin of Major Orders. *Mol. Biol. Evol.* **2011**, *28*, 1927–1942. [CrossRef] [PubMed]
44. Benson, D.A.; Cavanaugh, M.; Clark, K.; Karsch-Mizrachi, I.; Lipman, D.J.; Ostell, J.; Sayers, E.W. GenBank. *Nucleic Acids Res.* **2017**, *45*, D37–D42. [CrossRef] [PubMed]
45. Edgar, R.C. MUSCLE: A Multiple Sequence Alignment Method with Reduced Time and Space Complexity. *BMC Bioinform.* **2003**, *5*, 113. [CrossRef]
46. Swenson, N.G. *Functional and Phylogenetic Ecology in R*; Use R!; Springer: New York, NY, USA, 2014.
47. Peron, B. The energy landscape predicts flight height and wind turbine collision hazard in three species of large soaring raptor. *Mol. Biol. Evol.* **2017**, *10*, 512–526. [CrossRef]
48. Adams, D.C. Comparing Evolutionary Rates for Different Phenotypic Traits on a Phylogeny Using Likelihood. *Syst. Biol.* **2013**, *62*, 181–192. [CrossRef] [PubMed]
49. Weeks, B.C.; Naeem, S.; Winger, B.M.; Cracraft, J. The Relationship Between Morphology and Behavior in Mixed-Species Flocks of Island Birds. *Ecol. Evol.* **2020**, *10*, 10593–10606. [CrossRef]
50. Zuur, A.F.; Ieno, E.N.; Smith, G.M. *Analysing Ecological Data*; Statistics for Biology and Health; Springer: New York, NY, USA, 2007.